NSWCDD/TR-92/509

IMPROVED EMPIRICAL MODEL FOR BASE DRAG PREDICTION ON MISSILE CONFIGURATIONS BASED ON NEW WIND TUNNEL DATA

BY FRANK G. MOORE TOM HYMER
WEAPONS SYSTEMS DEPARTMENT

FLOYD J. WILCOX, JR.
NASA LANGLEY RESEARCH CENTER
HAMPTON, VA 23681-0001

OCTOBER 1992

NAVAL SURFACE WARFARE CENTER
DAHLGREN DIVISION
Dahlgren, Virginia 22448-5000

NSWCDD/TR-92/509

IMPROVED EMPIRICAL MODEL FOR BASE DRAG PREDICTION ON MISSILE CONFIGURATIONS BASED ON NEW WIND TUNNEL DATA

BY FRANK G. MOORE TOM HYMER
STRATEGIC SYSTEMS DEPARTMENT

FLOYD J. WILCOX, JR.
NASA LANGLEY RESEARCH CENTER
HAMPTON, VA 23681-0001

OCTOBER 1992

NAVAL SURFACE WARFARE CENTER
DAHLGREN DIVISION
Dahlgren, Virginia 22448-5000

FOREWORD

The effort described in this report is one part of the theoretical development necessary to make the last version of the Naval Surface Warfare Center Dahlgren Division (NSWCDD) Aeroprediction Code, published in 1981, more applicable to present and future weapon concepts. The particular theoretical development included in this report addresses the improvements needed for base drag prediction on missile configurations that may have combined effects of angle of attack and fin control deflection, fin location, and fin thickness.

Appreciation is expressed to NASA Langley Research Center (NASA/LRC) for its support in designing, building, and testing the wind tunnel model used for obtaining additional wind tunnel data. Acknowledgements are also given to Jim Bible and Sam Hardy of the Aeromechanics Branch, who provided some of the earlier wind tunnel model design ideas and wind tunnel test consultation.

The empirical base drag methodology developed in this report, along with partial cost of the wind tunnel model, was provided through the Office of Naval Research (Dave Siegel) and, more specifically, the Surface-launched Weapons Technology Block Program managed at NSWCDD by Robin Staton. Appreciation is expressed to these individuals for their support in this work.

Approved by:

David S. Malyevac

DAVID S. MALYEVAC
Deputy Department Head
Weapons Systems Department

ABSTRACT

New wind tunnel data have been taken, and a new empirical model has been developed for predicting base drag on missile configurations. The new wind tunnel data were taken at NASA/LaRC in the Unitary Plan Wind Tunnel at Mach numbers from 2.0 to 4.5, angles of attack to 16°, fin control deflections up to 20°, fin thickness-to- chord (t/c) ratio of 0.05 to 0.15, and fin locations flush with the base to two chord lengths upstream of the base.

The newly developed empirical model uses these data along with previous wind tunnel data. It estimates base drag as a function of all the above variables along with boattail and power-on or power-off effects. In comparing the new empirical model to that used in the former aeroprediction code, the new model gives improved accuracy compared to wind tunnel data. The new model also is more robust due to inclusion of additional variables. On the other hand, additional wind tunnel data are needed to validate or modify the current empirical model in areas where data are not available.

CONTENTS

ILLUSTRATIONS

ILLUSTRATIONS (CONTINUED)

ILLUSTRATIONS (CONTINUED)

1. INTRODUCTION

For the past 20 years, the Naval Surface Warfare Center Dahlgren Division has been involved in developing codes to calculate aerodynamics on tactical weapons. These codes have attempted to meet the changing needs of the Tactical Weapons Community and keep pace with aerodynamic requirements. A recent effort[1] was undertaken to look at where we have been, where we are, and where we need to go in the future with respect to aerodynamic codes. One of the primary needs identified in Reference 1 was an upgrade of the NSWCDD aeroprediction code to allow Mach numbers up to 20 (including the effects of real gases), improved lift prediction with particular emphasis on low aspect ratio lifting surfaces, and improved base drag prediction. All three of these efforts were undertaken. This report deals with the third of these objectives, providing improved base drag prediction capability for missile configurations.

The latest version of the aeroprediction code[2-4] (hereinafter referred to as Old Aeroprediction Code or OAP) calculates base drag empirically. It estimates the body-alone, zero angle-of-attack, power-off base drag using an average of wind tunnel data presented in several references.[5-13] These data assume a long cylindrical afterbody with a fully developed turbulent boundary layer ahead of the base. Figure 1 shows the base pressure coefficient currently used in the OAP as a function of Mach number. Deviations to this curve are expected due to Reynolds number, temperature, boattail or flare, angle of attack, fin thickness-to-chord (t/c) ratio, fin location, fin deflection, low body fineness ratio, or power on. [Note that Figure 1 also shows the Improved Aeroprediction Code (IAP) body-alone base pressure coefficient based on the present wind tunnel results, which will be discussed later.]

The methodology of References 2 through 4 neglects the effects of Reynolds number by assuming a Reynolds number combined with body roughness that is high enough to ensure fully developed turbulent flow at the base. Surface temperature effects are also neglected. The body is assumed to be at least 5 to 6 calibers long so that body fineness ratio effects are minimal. Also fin deflection effects were not accounted for due to lack of data. The body-alone, angle-of-attack base pressure coefficient change was estimated from Reference 7 and given in the OAP as

$$\left(\Delta C_{p_B}\right)_{NF,\alpha} = \left(C_{p_B}\right)_{NF,\alpha} - \left(C_{p_B}\right)_{NF,\alpha=0} = -(0.012 - 0.0036\,M_\infty)\,\alpha\,;\alpha \le 15^\circ \qquad (1)$$

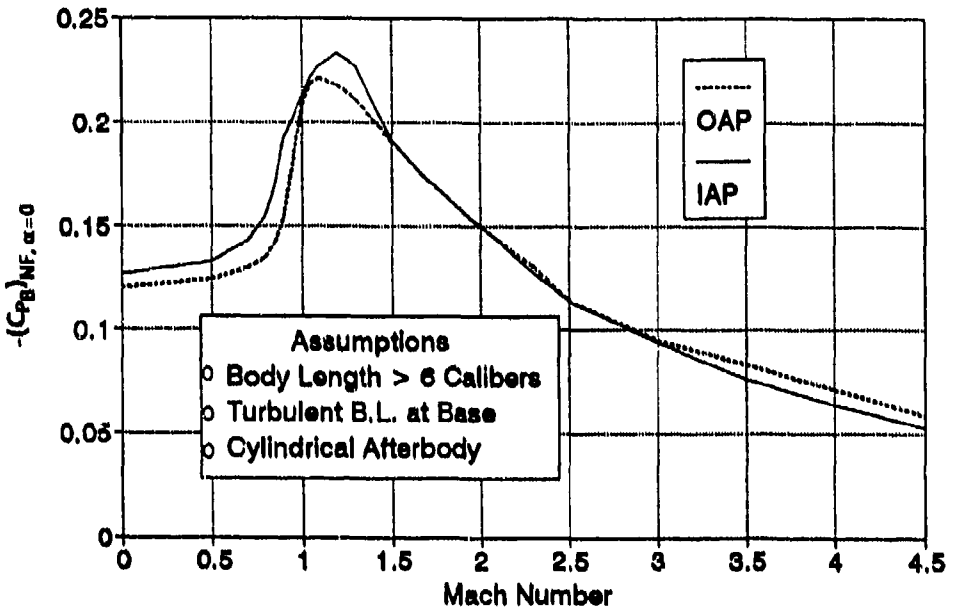

FIGURE 1. MEAN BODY-ALONE BASE PRESSURE COEFFICIENT USED IN OAP AND IAP

The base pressure was allowed to change up to an angle of attack of 15° and was held constant for angles of attack greater than this. The effects due to fin t/c ratio and fin location were estimated using the meager amount of data from References 14 through 16. Below $M_\infty = 1.5$, the effects were extrapolated to $M_\infty = 0$ based on judgment and some test data on configurations where the effects of fins could not clearly be separated from other effects. Figure 2 shows the change in the base pressure coefficient for various values of t/c ratio and Mach number that are in use in the OAP.

The effect of the location of the fins on base pressure was also estimated by use of the data in Reference 15. These data were interpolated in a linear sense (see Figure 3) as a function of fin t/c ratio according to

$$\frac{x}{c} = 10\ t/c \qquad (2)$$

where x is the distance from the base to the tail trailing edge ($\delta = 0°$) where the fin has no effect on base pressure. As an example, Equation (2) would indicate that the fin needs to be located one chord ahead of the base for a $t/c = 0.1$ fin to have no effect on base pressure. The fin effect on base pressure would therefore vary linearly from a maximum at $x/c = 0$ to zero for $x/c \geq 1.0$.

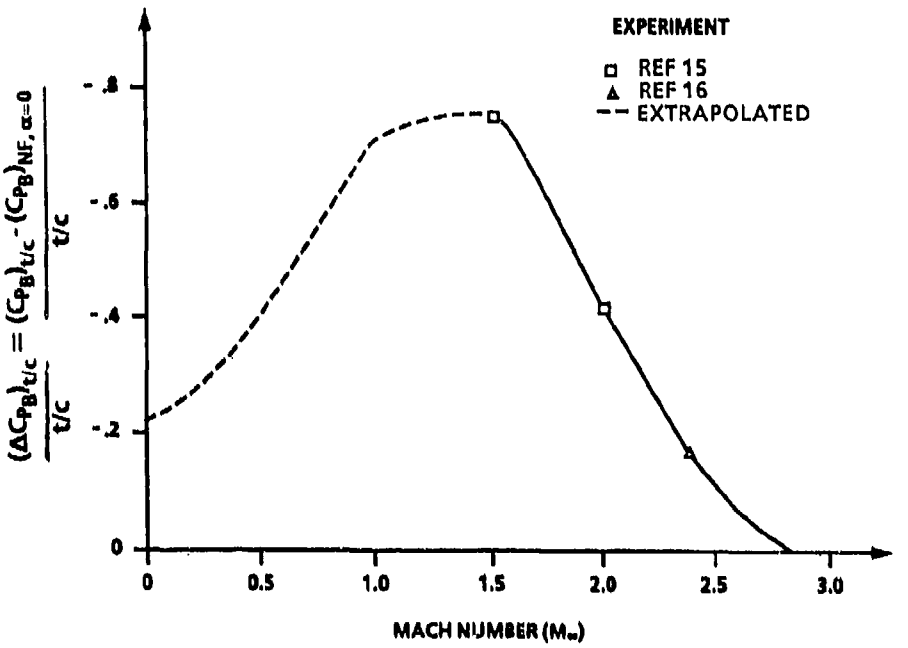

FIGURE 2. BASE PRESSURE COEFFICIENT CHANGE DUE TO t/c WITH FINS LOCATED FLUSH WITH BASE USED IN OAP

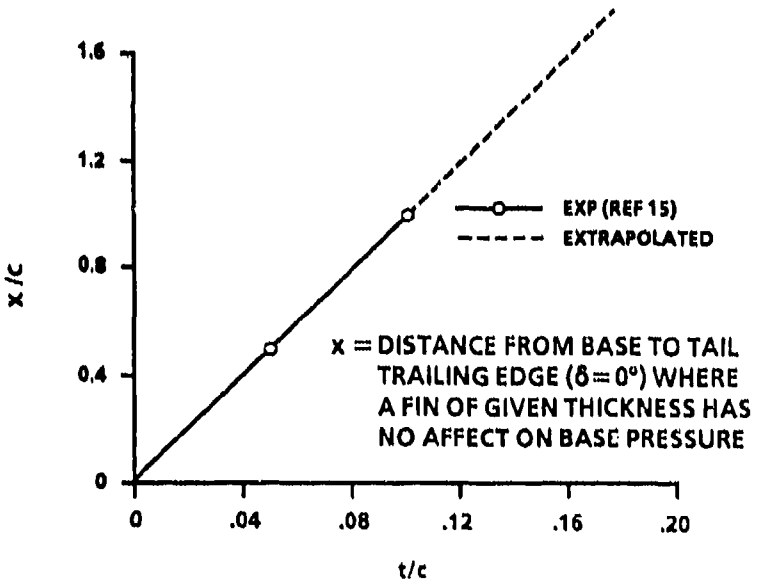

FIGURE 3. DISTANCE FROM BASE WHERE FINS DO NOT AFFECT BASE PRESSURE COEFFICIENT AS USED IN OAP

Finally, power-on effects were estimated by modifying the methodology of Brazzel[17,18] for higher values of mass flow at the nozzle exit. Also, boattail effects were estimated by the empirical data of Stoney[12] to give

$$C_{A_B} = - C_{p_B} \left(\frac{d}{d_{ref}} \right)^3 \tag{3}$$

Here, C_{p_B} includes all the effects just stated. For the details of the methodology and equations used, the interested reader is referred to References 19 and 20.

There are several problems with the methodology used in the OAP. All of these stem from the limited wind tunnel data available to estimate the change in base pressure as a function of the key parameters of interest. For most tactical missiles, it is believed that the neglect of Reynolds number, surface temperature, and body length-to-diameter ratio effects are acceptable so long as one remembers the constraints upon which these assumptions are made. Also, it is believed that the methodology in the OAP for inclusion of boattail and power-on effects are acceptable at present. However, estimates of the change in base pressure due to angle of attack, fin thickness, fin deflection, and fin location need to be improved upon or accounted for.

More specifically, the data for angle-of-attack effects were limited to small angles of attack ($\leq 10^0$) and Mach number. The data for fin location and t/c ratio were limited to $1.5 \leq M_\infty \leq 2.4$; $0 \leq t/c \leq 0.10$; $0 \leq x/c \leq 2.0$. It is well known that as Mach number gets high, base drag goes to zero. Hence, it is desirable to have base pressure measurements for $M_\infty < 5.0$; $\alpha \leq 30°$; $t/c \leq 0.15$; $x/c \leq 2.0$; and $\delta \leq 20°$. Also, data where a combination of these variables is investigated simultaneously is needed. Using these data, a more extensive and comprehensive empirical model to estimate base drag on missile configurations can be developed. While the data are needed for an improved base drag prediction model, they could also be very useful in validating Navier Stokes codes and in selecting appropriate turbulence models.

As a result of the need for additional wind tunnel test data, a request was made to NASA Langley Research Center (NASA/LaRC) to assist in providing such data. The data taken to date are for $2.0 \leq M_\infty \leq 4.5$, $\alpha \leq 16°$, $\delta \leq 20°$, $t/c \leq 0.15$, and $x/c \leq 2.0$. While these data are not as extensive as desired, they are by far the most extensive base drag database to date and will help in refining the empirical base drag prediction model of References 19 and 20. Hopefully, additional data at lower Mach numbers and higher angles of attack will be obtained in the future for additional refinements.

2. EXPERIMENTAL TESTS

2.1 MODEL DESCRIPTION

A photograph and drawing of the missile base pressure model are shown in Figure 4. The missile body was an ogive-cylinder 36 in. long and 5.0 in. in diameter. Four cruciform aft tail fins could be attached to the missile body in a plus orientation at three longitudinal locations. At each longitudinal location, the fin incidence could be set at 0°, 10°, and 20°. Three sets of fins were tested that had the same planform but varied in thickness. The base was instrumented with 89 pressure orifices that were arranged along radial lines at 22.5° increments and 7 constant radiuses from the center of the base.

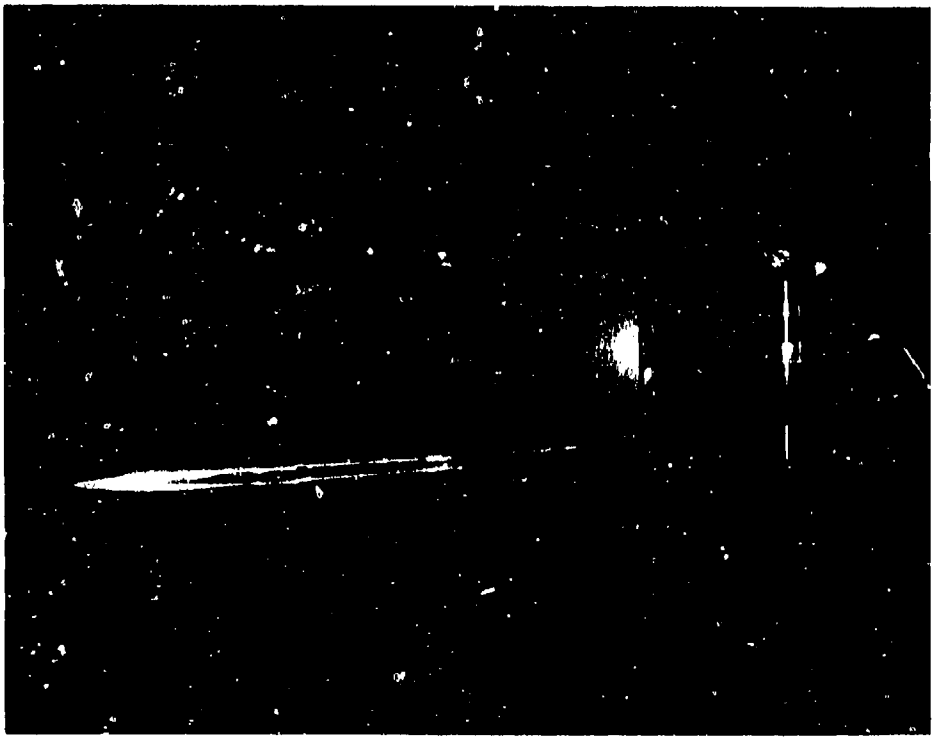

a. MODEL MOUNTED IN WIND TUNNEL

FIGURE 4. MISSILE BASE PRESSURE MODEL DESCRIPTION

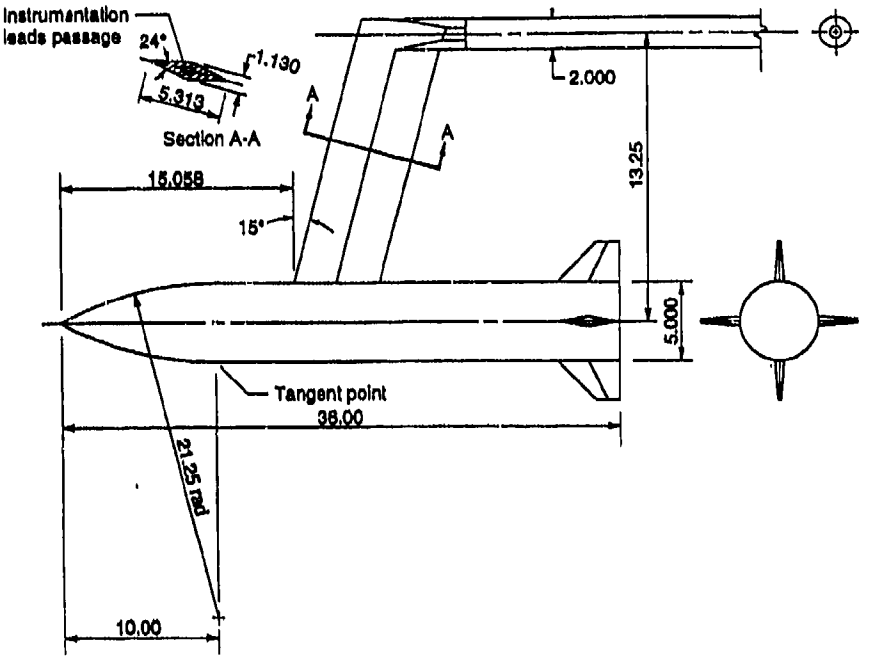

b. BODY AND SUPPORT STRUT DETAILS

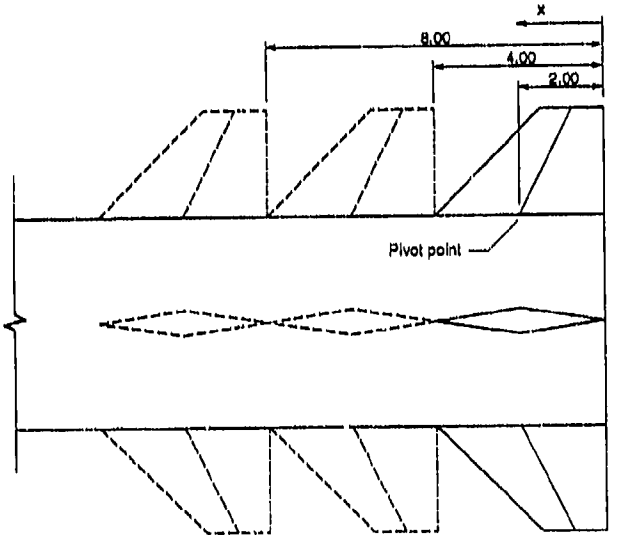

x	x/c
0	0
4.00	1.0
8.00	2.0

c. LONGITUDINAL FIN LOCATIONS

FIGURE 4. MISSILE BASE PRESSURE MODEL DESCRIPTION (CONTINUED)

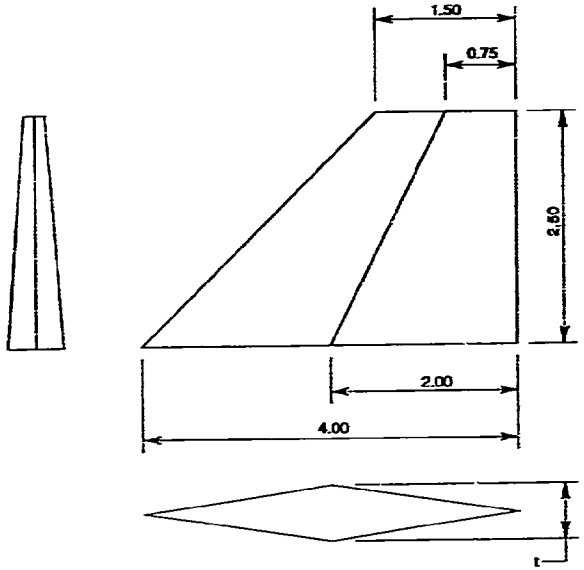

t	t/c	t_{tip}
0.20	0.05	0.075
.40	.10	.150
.50	.15	.225

d. FIN DETAILS

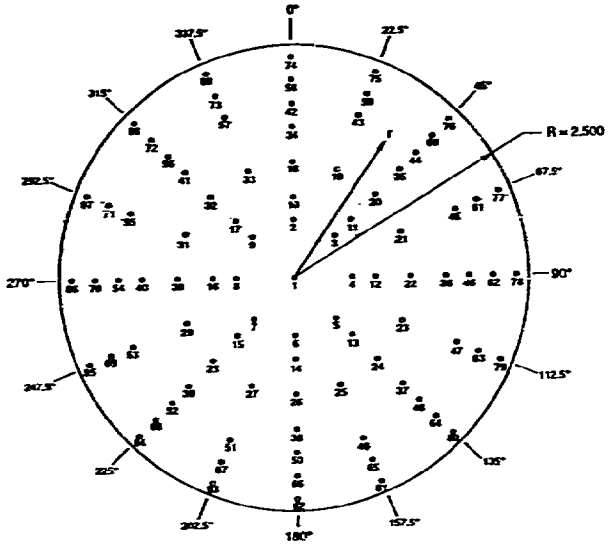

Pressure orifices located at the following:

r	r/R
0	0
0.625	0.25
.975	.35
1.250	.5
1.625	.65
1.875	.75
2.125	.85
2.375	.95

e. BASE PRESSURE ORIFICE LOCATIONS

FIGURE 4. MISSILE BASE PRESSURE MODEL DESCRIPTION (CONTINUED)

The model was attached to a vertical strut near the middle of the missile body on the upper surface (leeward side of model as α increases). The strut had a diamond cross section and was swept 15°. The strut leading edge wedge half-angle was 12° and was sufficiently small to maintain an attached shock on the leading edge at the lowest Mach number tested and at small angles of attack. At larger angles of attack, the strut was on the leeward side of the missile body and would have minimal influence on the missile base pressure. The top of the strut was sufficiently far from the model centerline (19.25 in.) so that a Mach line emanating from the top leading edge of the strut would not intersect a tail fin on the model and would intersect the model centerline at least 1.5 body diameters downstream of the model base at the lowest Mach number tested. The strut was attached to the tunnel model support system through a 90°-offset sting holder that allowed the vertical position of the model to be varied in the test section. The model nose was typically slightly below the tunnel centerline to increase the maximum attainable angle of attack and provide clearance at the tunnel ceiling to ensure that the strut was outside of the tunnel wall boundary layer to minimize possible boundary layer separation and tunnel flow breakdown.

2.2 WIND TUNNEL TESTS

The wind tunnel tests were conducted in the NASA/LaRC Unitary Plan Wind Tunnel (UPWT), which is a continuous flow, variable pressure supersonic wind tunnel with a Mach number range of 1.5 to 4.6. The tunnel has two test sections, each of which covers only part of the Mach number range; the low Mach number test section has a range of 1.5 to 2.9, and the high Mach number test section has a range of 2.4 to 4.6. The test sections are approximately 4 ft square by 7 ft long. The nozzle ahead of each test section consists of an asymmetric sliding block that allows a continuous variation of Mach number while the tunnel is in operation. A complete description of the tunnel and test section calibration information is presented in a NASA report.[21]

The tests were conducted at the following conditions:

M_∞	R_n (1 / ft)	p_0 (lb / ft2)	T_0 (°F)	q (lb / ft2)
2.0	2×10^6	1253	125	449
2.5	2×10^6	1600	125	410
3.0	2×10^6	2216	150	380
3.5	2×10^6	2882	150	324
4.0	2×10^6	3698	150	273
4.5	2×10^6	4666	150	229

The dew point in the tunnel was maintained sufficiently low at all test conditions to ensure negligible water condensation effects. The model angle of attack was varied from 0° to approximately 16° for tests conducted in the high Mach number test section ($M_\infty \geq 2.5$) and from 0° to approximately 10° for tests conducted in the low Mach number test section ($M_\infty = 2.0$).

The tunnel flow angularity was determined by measuring the pressure difference between two orifices located 180° apart in a vertical plane on the missile nose as the model was run through a small angle of attack range. These pressure differences were plotted against the model attitude which was referenced to the horizontal. A least-squares fit was applied to the data and the tunnel flow angularity at a given Mach number was the angle at which the pressure difference was zero. This procedure was performed at all Mach numbers and all the data were corrected for tunnel flow angularity.

To ensure a turbulent boundary layer over the model, transition grit was applied to the missile nose and to the leading edge of each fin. The transition strips were located 1.8 in. from the model nose measured along the model surface and 0.6 in. from the fin leading edges measured streamwise. For $M_\infty \geq 2.5$, the transition strips consisted of #35 sand grit (0.0215±0.0018 in.) individually spaced 0.09 in. apart on the model nose and 0.12 in. apart measured parallel to the fin leading edges. For $M_\infty = 2.0$, the transition strips consisted of #45 sand grit (0.0152±0.0013 in.) sparsely sprinkled in a lacquer film. The size and location of the transition grit was determined from documented procedures[22] except that a critical roughness Reynolds number of 1800 was used instead of the recommended value of 600. The increase in critical roughness Reynolds number above the recommended value was due to the effects of high Mach number and was determined using guidance from a NASA publication[23] and unpublished data obtained in the UPWT.

2.3 MEASUREMENTS AND DATA

The pressures on the model were measured with two electronically scanned pressure modules that were located inside the model. The modules had a full-scale range of ±5 psid. All 89 pressure orifices on the model base were measured simultaneously for each data point. The model angle of attack was measured with an accelerometer that was mounted inside the missile body.

The missile base drag coefficient was calculated using an area weighted average of the base pressure coefficients as shown in the following equation.

$$C_{D_B} = -C_{p_1}\left(\frac{A_1}{A}\right) + \sum_{i=2}^{9}\left[-C_{p_i}\left(\frac{A_2}{A}\right)\right] + \sum_{i=10}^{17}\left[-C_{p_i}\left(\frac{A_3}{A}\right)\right]$$

$$+ \sum_{i=18}^{33}\left[-C_{p_i}\left(\frac{A_4}{A}\right)\right] + \sum_{i=34}^{41}\left[-C_{p_i}\left(\frac{A_5}{A}\right)\right] + \sum_{i=42}^{57}\left[-C_{p_i}\left(\frac{A_6}{A}\right)\right] \qquad (4)$$

$$+ \sum_{i=58}^{73}\left[-C_{p_i}\left(\frac{A_7}{A}\right)\right] + \sum_{i=74}^{89}\left[-C_{p_i}\left(\frac{A_8}{A}\right)\right]$$

where

C_{p_i} = pressure coefficient corresponding to orifice i
i = orifice number
A = base area
$A_1, A_2, \ldots, A_8$ = area used as weighting factor

Tests were conducted both with and without tail fins. Data were obtained at discrete α for cases with tail fins and over a range of α for cases without tail fins. A complete description of all the configurations that were tested is contained in Table 1. Table 2 contains a list of the base drag data.

Two problems arose during this test that affected the uncertainty of the measured pressure data using the electronically scanned pressure modules. The first problem was model vibrations, which were possibly caused by either normal tunnel vibrations being transmitted through the long-cantilevered sting/strut or aerodynamic flow unsteadiness which caused the model and sting/strut to vibrate. The model was not instrumented to determine the exact cause of the vibrations. The second problem was temperature variations inside the model that were primarily caused by the variation of tunnel stagnation temperature as the tunnel was brought online to the desired test conditions. Because no data were specifically obtained to determine the experimental data uncertainty caused by model vibrations and temperature variations, the pressure data uncertainty was estimated from data obtained during routine checks of the pressure instrumentation to ensure data system integrity. The checks consisted of either applying a known pressure to the modules on all the pressure ports and comparing the module reading to a standard pressure gauge or calibrating the module on-line[24] and comparing data points taken before and after the calibration. Using the data from these checks, the base drag coefficients are estimated to have an uncertainty of approximately ±5 percent of the calculated values.

TABLE 1. CONFIGURATION INDEX

Configuration	t/c				x/c					δ					α ($M_\infty = 2.0$)	α ($M_\infty \geq 2.5$)
	Fins off	.05	.10	.15	.5	1.0	1.5	2.0	2.5	0	5	10	15	20		
1	X														sweep	sweep
2				X	X					X					0,5,10	0
3				X	X							X			0,5,10	0
4				X	X									X	0,5,10	0
5			X		X					X					0,5,10	0
6			X		X							X			0,5,10	0
7			X		X									X	0,5,10	0
8		X			X					X					0,5,10	0
9		X			X							X			0,5,10	0
10		X			X									X	0,5,10	0
11		X					X			X					0,5,10	0
12			X				X			X					0,5,10	0
13				X			X			X					0,5,10	0
14				X					X	X					0,5,10	0
15			X						X	X					0,5,10	0
16		X							X	X					0,5,10	no data

TABLE 2. BASE PRESSURE COEFFICIENT DATA

Configuration	M_∞	α	C_{D_B}
1	2.0	0.0	0.138
1	2.0	2.0	0.151
1	2.0	4.0	0.172
1	2.0	6.0	0.192
1	2.0	8.0	0.207
1	2.0	10.0	0.218
1	2.0	12.3	0.231
1	2.5	0.0	0.106
1	2.5	2.0	0.119
1	2.5	4.0	0.136
1	2.5	6.0	0.148
1	2.5	8.0	0.157
1	2.5	10.0	0.165
1	2.5	12.0	0.160
1	2.5	14.0	0.156
1	2.5	15.0	0.154
1	2.5	15.8	0.149
1	3.0	0.0	0.090
1	3.0	2.0	0.099
1	3.0	4.0	0.109
1	3.0	6.0	0.117
1	3.0	8.0	0.123
1	3.0	10.0	0.129
1	3.0	12.0	0.119
1	3.0	14.0	0.118
1	3.0	15.0	0.118
1	3.0	16.1	0.121
1	3.5	0.0	0.080
1	3.5	2.0	0.086
1	3.5	4.0	0.091
1	3.5	6.0	0.096
1	3.5	8.0	0.099
1	3.5	10.0	0.096
1	3.5	12.0	0.094
1	3.5	14.0	0.095
1	3.5	15.0	0.094
1	3.5	15.6	0.094
1	4.0	0.0	0.065
1	4.0	2.0	0.068
1	4.0	4.0	0.073
1	4.0	6.0	0.076
1	4.0	8.0	0.077
1	4.0	10.0	0.074
1	4.0	12.0	0.074
1	4.0	14.0	0.074
1	4.0	15.0	0.074
1	4.0	16.1	0.074

Configuration	M_∞	α	C_{D_B}
1	4.5	0.0	0.053
1	4.5	2.0	0.056
1	4.5	4.0	0.058
1	4.5	6.0	0.061
1	4.5	8.0	0.060
1	4.5	10.0	0.059
1	4.5	12.0	0.059
1	4.5	14.0	0.059
1	4.5	15.0	0.058
1	4.5	16.0	0.057
2	2.0	0.0	0.167
2	2.0	5.0	0.190
2	2.0	10.0	0.210
2	2.5	0.0	0.136
2	3.0	0.0	0.114
2	3.5	0.0	0.092
2	4.0	0.0	0.073
2	4.5	0.0	0.058
3	2.0	0.0	0.194
3	2.0	5.0	0.204
3	2.0	10.0	0.219
3	2.5	0.0	0.150
3	3.0	0.0	0.118
3	3.5	0.0	0.094
3	4.0	0.0	0.075
3	4.5	0.0	0.061
4	2.0	0.0	0.224
4	2.0	5.0	0.223
4	2.0	10.0	0.227
4	2.5	0.0	0.161
4	3.0	0.0	0.122
4	3.5	0.0	0.095
4	4.0	0.0	0.075
4	4.5	0.0	0.061
5	2.0	0.0	0.158
5	2.0	5.0	0.184
5	2.0	10.0	0.208
5	2.5	0.0	0.127
5	3.0	0.0	0.108
5	3.5	0.0	0.089
5	4.0	0.0	0.071
5	4.5	0.0	0.058
6	2.0	0.0	0.188
6	2.0	5.0	0.197
6	2.0	10.0	0.213
6	2.5	0.0	0.146
6	3.0	0.0	0.117
6	3.5	0.0	0.094
6	4.0	0.0	0.075
6	4.5	0.0	0.061

TABLE 2. BASE PRESSURE COEFFICIENT DATA (CONTINUED)

Configuration	M_∞	α	C_{D_B}
7	2.0	0.0	0.219
7	2.0	5.0	0.221
7	2.0	10.0	0.226
7	2.5	0.0	0.160
7	3.0	0.0	0.121
7	3.5	0.0	0.095
7	4.0	0.0	0.074
7	4.5	0.0	0.059
8	2.0	0.0	0.148
8	2.0	5.0	0.174
8	2.0	10.0	0.204
8	2.5	0.0	0.116
8	3.0	0.0	0.100
8	3.5	0.0	0.084
8	4.0	0.0	0.067
8	4.5	0.0	0.054
9	2.0	0.0	0.185
9	2.0	5.0	0.193
9	2.0	10.0	0.210
9	2.5	0.0	0.141
9	3.0	0.0	0.113
9	3.5	0.0	0.091
9	4.0	0.0	0.072
9	4.5	0.0	0.058
10	2.0	0.0	0.216
10	2.0	5.0	0.217
10	2.0	10.0	0.225
10	2.5	0.0	0.155
10	3.0	0.0	0.120
10	3.5	0.0	0.093
10	4.0	0.0	0.073
10	4.5	0.0	0.057
11	2.0	0.0	0.138
11	2.0	5.0	0.158
11	2.0	10.0	0.192
11	2.5	0.0	0.109
11	3.0	0.0	0.090
11	3.5	0.0	0.079
11	4.0	0.0	0.064
11	4.5	0.0	0.052
12	2.0	0.0	0.139
12	2.0	5.0	0.158
12	2.0	10.0	0.190
12	2.5	0.0	0.113
12	3.0	0.0	0.096
12	3.5	0.0	0.083
12	4.0	0.0	0.067
12	4.5	0.0	0.054

Configuration	M_∞	α	C_{D_B}
13	2.0	0.0	0.141
13	2.0	5.0	0.160
13	2.0	10.0	0.188
13	2.5	0.0	0.121
13	3.0	0.0	0.103
13	3.5	0.0	0.087
13	4.0	0.0	0.068
13	4.5	0.0	0.055
14	2.0	0.0	0.143
14	2.0	5.0	0.172
14	2.0	10.0	0.207
14	2.5	0.0	0.116
14	3.0	0.0	0.100
14	3.5	0.0	0.084
14	4.0	0.0	0.068
14	4.5	0.0	0.055
15	2.0	0.0	0.141
15	2.0	5.0	0.171
15	2.0	10.0	0.208
15	2.5	0.0	0.112
15	3.0	0.0	0.095
15	3.5	0.0	0.082
15	4.0	0.0	0.066
15	4.5	0.0	0.054
16	2.0	0.0	0.139
16	2.0	5.0	0.168
16	2.0	10.0	0.207

3. EMPIRICAL MODEL FOR BASE DRAG PREDICTION

3.1 BODY-ALONE CONFIGURATION

Using the wind tunnel data of Tables 1 and 2, the percent change in the body-alone base pressure coefficient was calculated as a function of angle of attack, and these results are given in Figure 5a for Mach numbers $2.0 \leq M_\infty \leq 4.5$. Note that no data are available above $M_\infty = 4.5$, so a linear extrapolation indicates no change in base pressure with angle of attack above $M_\infty = 5.5$. Also, no data could be taken for angles of attack greater than about 15° because the model support strut would have hit the tunnel ceiling. For higher angles of attack, the data for $M_\infty \geq 2.5$ show an angle of attack where the base pressure increase is a maximum and then a gradual decline with further increases in α. This general trend was assumed for all results in both Figures 5a and b until additional high angle-of-attack data are made available. The large NASA Tri Service Data Base[25] was investigated for inclusion of high angle-of-attack pressure effects. However, the emphasis in those tests was on lifting properties, and the axial force was of secondary concern. Hence, while axial force and base pressure information is available, the accuracy of the base pressure information is not believed to be as good as desired for use here.

For Mach numbers below 2, the data of Reference 26 were used to obtain the change in base pressure due to angle of attack. These results are given in Figure 5b. In contrast to Reference 25, this test did concentrate on axial force information. The Reynolds number of the transonic portion of the test was also high enough to ensure a turbulent boundary layer at the base for Mach numbers less than 1.5. However, only three base pressure taps were mounted on the base of the model, and a sting was also in place. Hence, the data are probably not of the same quality as that of the more recent data in this report where numerous pressure taps were available to get a more accurate average of base pressure.

It should be pointed out that both Figures 5a and 5b are given in percent change in the body-alone base pressure coefficient as a function of angle of attack. These curves were obtained using data from Table 2 and Figure 1 for $2.0 \leq M_\infty \leq 4.5$ and Reference 26 for $0.6 \leq M_\infty \leq 1.5$. The quantity F_1 was calculated by subtracting the body-alone value of C_{p_B} at $\alpha = 0°$ (from Table 2 or Reference 26) from the body-alone value of C_{p_B} at some α (from Table 2 or Reference 26) and dividing this quantity by the body-alone value of C_{p_B} at $\alpha = 0°$ from Figure 1. This method of nondimensionalizing the change in C_{p_B} of the present experimental data with the C_{p_B} at $\alpha = 0°$ from Figure 1 compensates for the slight difference between the body-alone value of C_{p_B} at $\alpha = 0°$ from Figure 1 and Table 2 of Reference 26. It should be emphasized that throughout this section describing the derivation of the empirical base drag prediction model, the body-alone value of C_{p_B} at $\alpha = 0°$ ($(C_{p_B})_{NF,\alpha=0°}$) used to nondimensionalize the changes in the present experimental data was obtained from Figure 1.

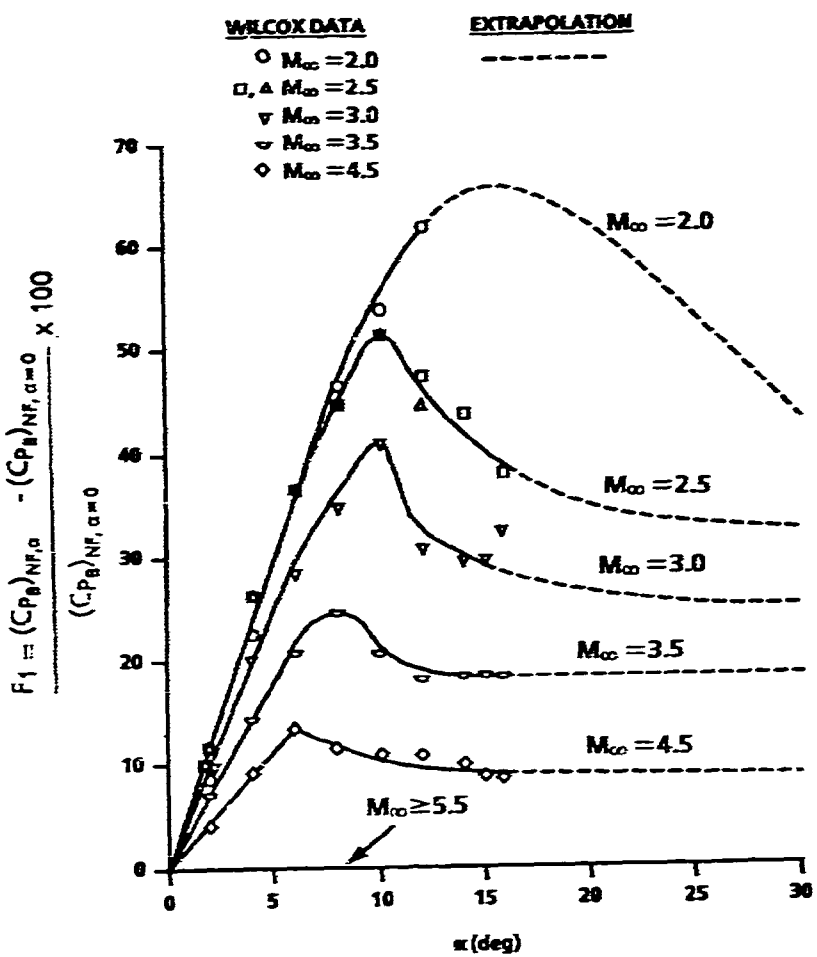

FIGURE 5a. PERCENT INCREASE IN BODY-ALONE BASE PRESSURE COEFFICIENT DUE TO ANGLE OF ATTACK ($M_\infty \geq 2$)

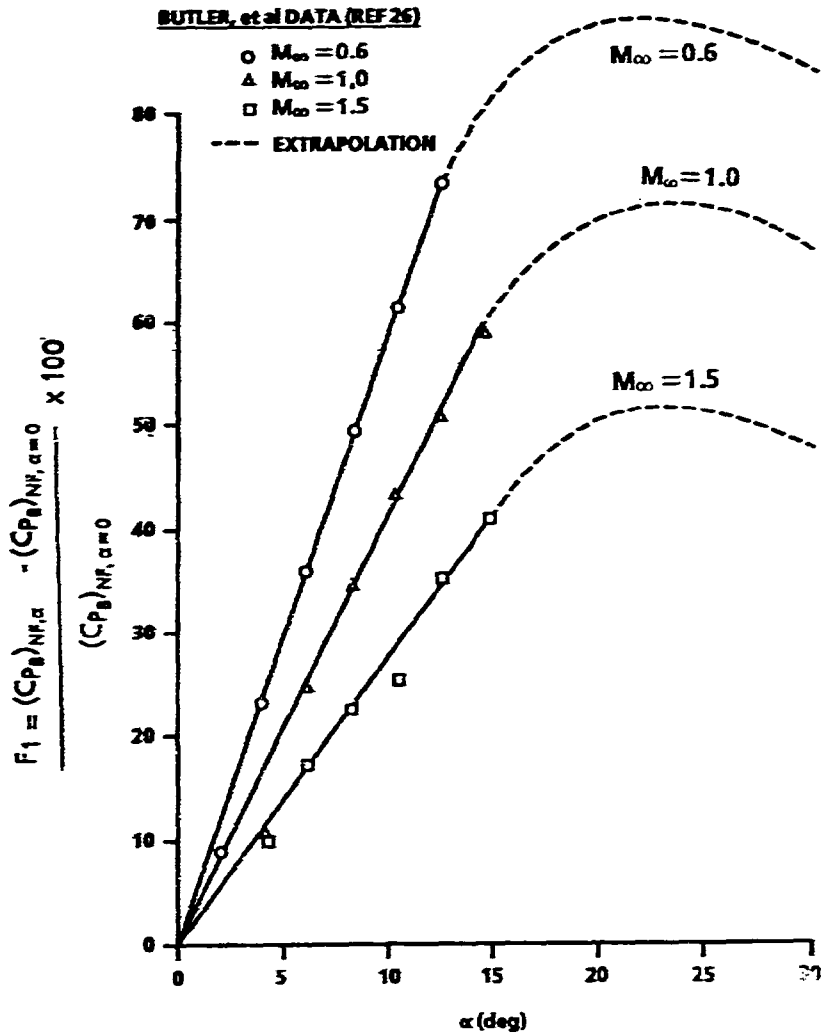

FIGURE 5b. PERCENT INCREASE IN BODY-ALONE BASE PRESSURE COEFFICIENT DUE TO ANGLE OF ATTACK ($M_\infty < 2$)

In viewing Figures 5a and b, it is evident that angle of attack has a strong effect on base pressure and hence base drag. It is also evident that additional wind tunnel data are needed for angles of attack greater than 15° at $M_\infty \leq 4.5$.

The base pressure coefficient and drag of the body-alone configuration is then estimated as

$$\left(C_{P_B}\right)_{NF,\alpha} = \left(C_{P_B}\right)_{NF,\alpha=0} \left| 1 + 0.01\, F_1 \right| \tag{5}$$

and

$$C_{A_B} = -\left(C_{P_B}\right)_{NF,\alpha} \left(\frac{d}{d_{ref}}\right)^3 \tag{5a}$$

where $(C_{P_B})_{NF,\alpha=0}$ comes from the IAP results of Figure 1 and F_1 from Figures 5a and b. Note that the recent data of this report and the Reference 26 data allowed slight revisions of the OAP results for $(C_{P_B})_{NF,\alpha=0}$ as seen in Figure 1.

If the engine is in a power-on mode, the base pressure coefficient at $\alpha=0$ will be modified according to References 16 and 17 as currently done in the OAP.

3.2 BODY-TAIL CONFIGURATION

There are three significant base pressure effects that need to be accounted for on missiles having tail surfaces located near the base. These include fin deflection, fin thickness, and fin location. Fin planform shape and aspect ratio also are design parameters of interest. However, they will not be modeled in the present empirical methodology. As seen in the Section 2 discussion on the wind tunnel test, a double wedge airfoil section was used for all tests. The fin planforms had a constant aspect ratio of 1.82 and the fin trailing edges were sharp. The planform shape chosen was thus fairly typical of missile tail fin planforms both in aspect ratio and airfoil section.

The first effect to consider is control deflection. Initially, it was hoped that body angle of attack and fin control deflection could be separated and modeled separately. However, it became clear that this was not possible for two reasons: (1) more data were needed than were acquired in the test and (2) based on the limited amount of data available, it appeared that angle of attack and control deflection were closely coupled. As a result, when fins were present, the empirical model arrived at a curve that gave the percent increase in base pressure coefficient as a function of the absolute value of $\alpha+\delta$ based on the limited amount of data available. To arrive at this curve, it was first necessary to determine the increase in base pressure due to fin deflection for zero thickness fins. This was done by taking the data for the three values of t/c available and extrapolating to $t/c=0$. An example of this is shown in Figure 6 for $M_\infty=2$ at $x/c=0$. At this Mach number, both angle of attack and control deflection data were available for each value of t/c from 0.05 to 0.15. For other Mach

numbers, only control deflection data were available at x/c = 0. As seen in Figure 6, the change in base pressure due to fin deflection or body angle of attack varies nearly linearly with fin t/c ratio making it easy to pick off the value of ΔC_{P_B} due to fin deflection or body angle of attack at t/c = 0. Figure 7 presents the entire data set of increase in base pressure at t/c = 0 as a function of $|\alpha+\delta|$. Here, the figure has been nondimensionalized by the value of the body-alone base pressure coefficient (obtained from Figure 1) and given as a percentage increase. A linear extrapolation of the data above $M_\infty = 4.5$ indicates that there is no increase at $M_\infty = 5.5$. However, no accurate data are known to be available for $M_\infty < 2$, so the curve for $M_\infty = 2$ is assumed to hold below $M_\infty = 2$. It should be pointed out that this is one reason that the empirical model was derived in terms of percent increase in base pressure coefficient relative to the body-alone base pressure coefficient at $\alpha = 0$. This way, even though no data for control deflection effects are available below $M_\infty = 2$, we still know $(C_{P_B})_{NF,\ \alpha=0}$ fairly accurately for the body alone; hence, it is believed that the assumption of using the curve in Figure 7 to represent the percent increase in base pressure due to fin deflection is better than trying to derive a model based on the value of ΔC_{P_B} due to fin deflection The only assumption in Figure 7 is therefore the shape of the curve at $M_\infty = 2$ is assumed to apply below $M_\infty = 2$.

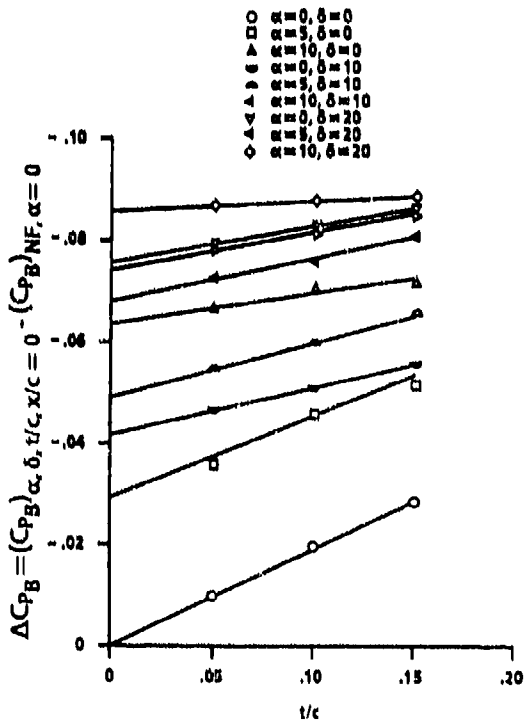

FIGURE 6. EFFECTS OF ANGLE OF ATTACK AND CONTROL DEFLECTION ON BASE PRESSURE COEFFICIENT ($M_\infty = 2$, x/c = 0)

It is apparent in viewing Figure 7 that additional wind tunnel data are needed for control deflection and body angle of attack below $M_\infty=2$ as well as combined values of $|\alpha+\delta|$ at $M_\infty>2$ in order to have a more accurate estimate of percent increase in base pressure coefficient due to control deflection. However, until additional data become available, Figure 7 will be the model used in the IAP.

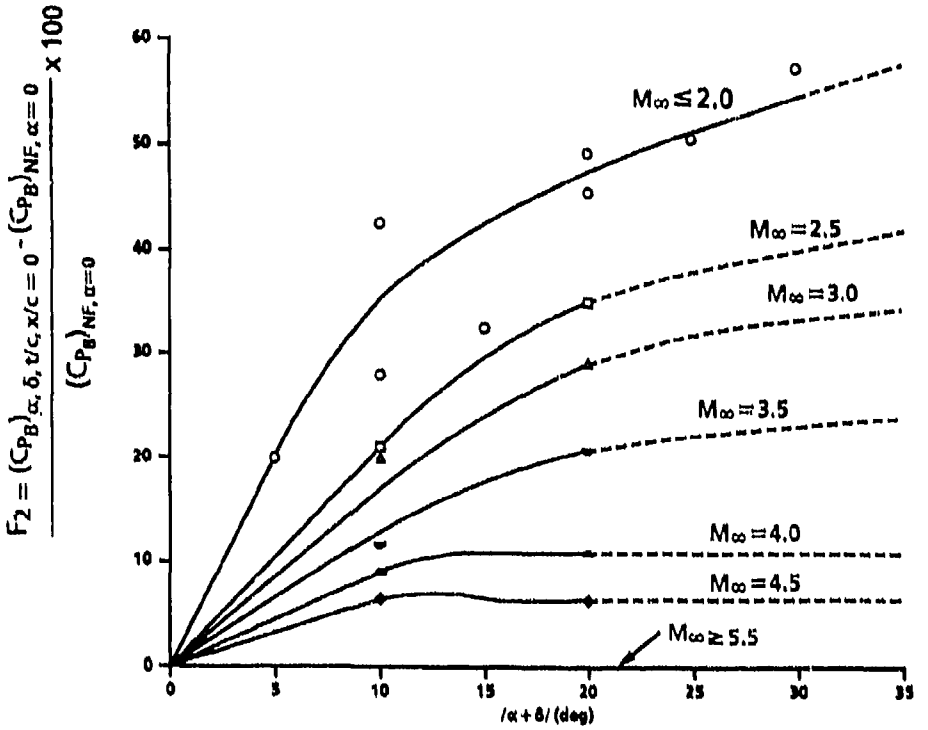

FIGURE 7. PERCENT INCREASE IN BASE PRESSURE COEFFICIENT DUE TO COMBINED EFFECTS OF ANGLE OF ATTACK AND CONTROL DEFLECTION (t/c ≃0)

The next parameter of interest is fin thickness effects on base pressure. Most references (see for example 14 and 15), including the OAP model, estimate the change in base pressure as a function of fin t/c ratio. However, in plotting data from several sources, see Figure 8a, it appeared that t/c may not be the most appropriate parameter. Fin thickness-to-body diameter (t/d) was also investigated (see Figure 8b) and this appeared to be a much more appropriate way to approximate fin thickness since the data of Figure 8a was coellesed in a much smoother curve in Figure 8b. As a result, the empirical model of fin thickness effects on base pressure will be derived on the basis of t/d versus t/c.

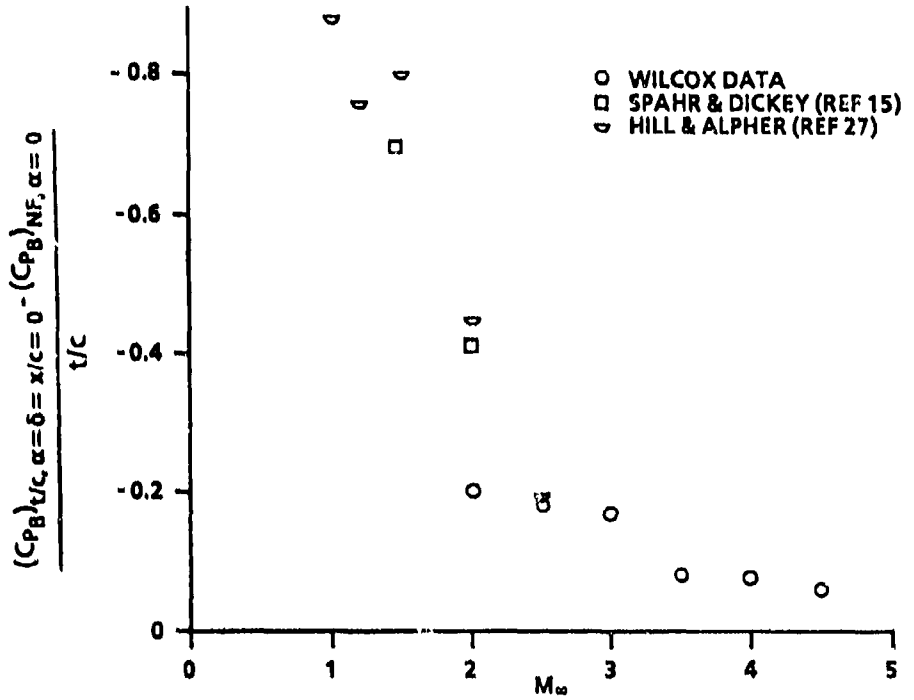

FIGURE 8a. EFFECTS OF FIN t/c RATIO ON BASE PRESSURE COEFFICIENT ($x/c = \alpha = \delta = 0$)

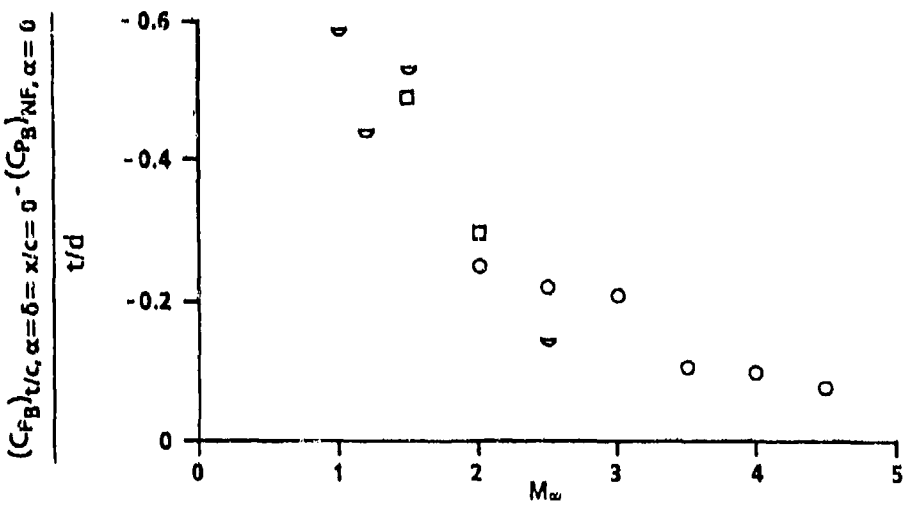

FIGURE 8b. EFFECTS OF FIN t/d RATIO ON BASE PRESSURE COEFFICIENT ($x/c = \alpha = \delta = 0$)

In analyzing the data of the present report, it also became clear that fin thickness was an important parameter at low angle of attack and control deflection but became less important at larger values of $|\alpha+\delta|$. That is, given the increase of C_{P_B} due to $|\alpha+\delta|$ from Figure 7, the additional increase in C_{P_B} due to fin thickness decreased with increasing $|\alpha+\delta|$. These results are shown in Figure 9, which gives the additional percent increase in base pressure due to fin t/d ratio as a function of Mach number and $|\alpha+\delta|$. Once again, additional data are needed, in particular for Mach numbers less than 2. For $|\alpha+\delta| = 0$, the data of Reference 27 supplements the present data down to $M_\infty = 1$. Until additional data are available, the trend of F_3 below $M_\infty = 1$ is assumed to be similar to that of the base pressure coefficient curve of Figure 1. Also, for values of $|\alpha+\delta| \geq 30°$, fin thickness effects on base pressure are assumed to be zero.

The total body base pressure coefficient for fins located flush with the base is then

$$\left(C_{P_B}\right)_{\alpha,\,\delta,\,t/c,\,x/c=0} = \left(1 + 0.01\,F_2\right)\left(C_{P_B}\right)_{NF,\,\alpha=0} + 0.01\,F_3(t/d) \qquad (6)$$

where $(C_{P_B})_{NF,\,\alpha=0}$, F_2, and F_3 come from the IAP curve of Figure 1 and Figures 7 and 9, respectively.

The final parameter to model is fin location effects relative to the body base. Figure 10 shows the percent change in base pressure coefficient for various angles of attack and t/d values as a function of x/c for $M_\infty = 2$. This figure was based on the new wind tunnel data of Tables 1 and 2. Note that at $\alpha = 0$, Figure 10a, (taken here to be $|\alpha+\delta|$), ΔC_{p_B} goes close to zero about a caliber or so ahead of the base. Also note that the ΔC_{p_B} of Figure 10 is the change in base pressure at a given angle of attack due to the presence of the fins.

On the other hand, examining Figures 10b and c, it is seen that as α or $|\alpha+\delta|$ becomes appreciable, the fins need to be located about 2.5 calibers ahead of the base before the fin effects are minimal and the body angle-of-attack effect is the dominant factor.

Also, it is noted that the percent change in base pressure coefficient in Figure 10 for $\alpha = 5$ and 10° initially has a negative slope similar to the $\alpha = 0$ case but then reverses and approaches no change at $x/c = 2.5$. As a result, a numerical interpolation is used to compute the percent change in ΔC_{P_B} as a function of x/c, $|\alpha+\delta|$, and t/d. This same percent change is assumed to occur at all Mach numbers since no data are available other than at $M_\infty = 2$.

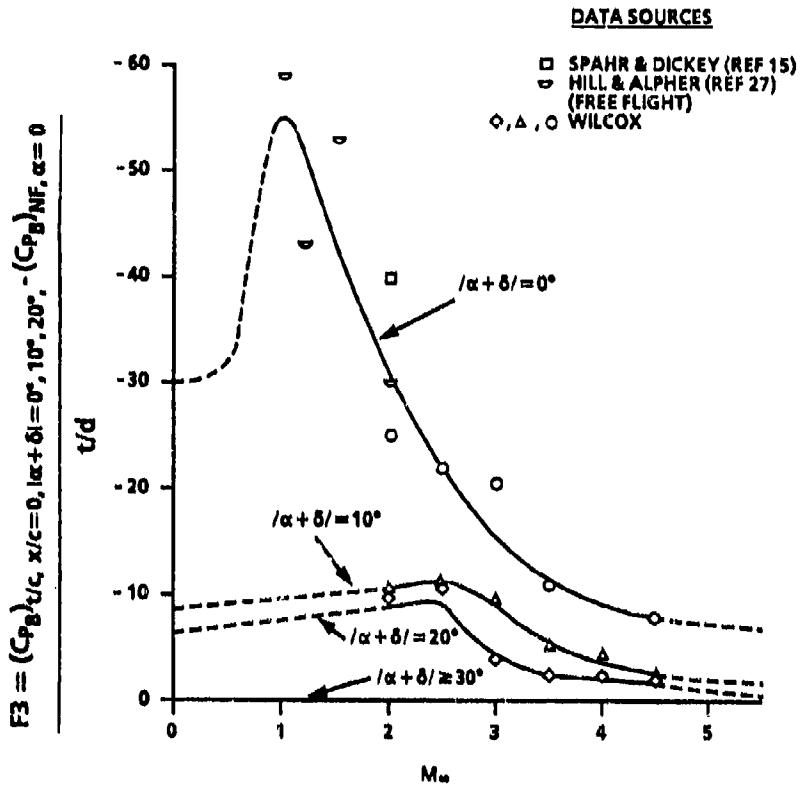

FIGURE 9. PERCENT INCREASE IN BASE PRESSURE COEFFICIENT DUE TO FIN THICKNESS AT VARIOUS VALUES OF $|\alpha+\delta|$

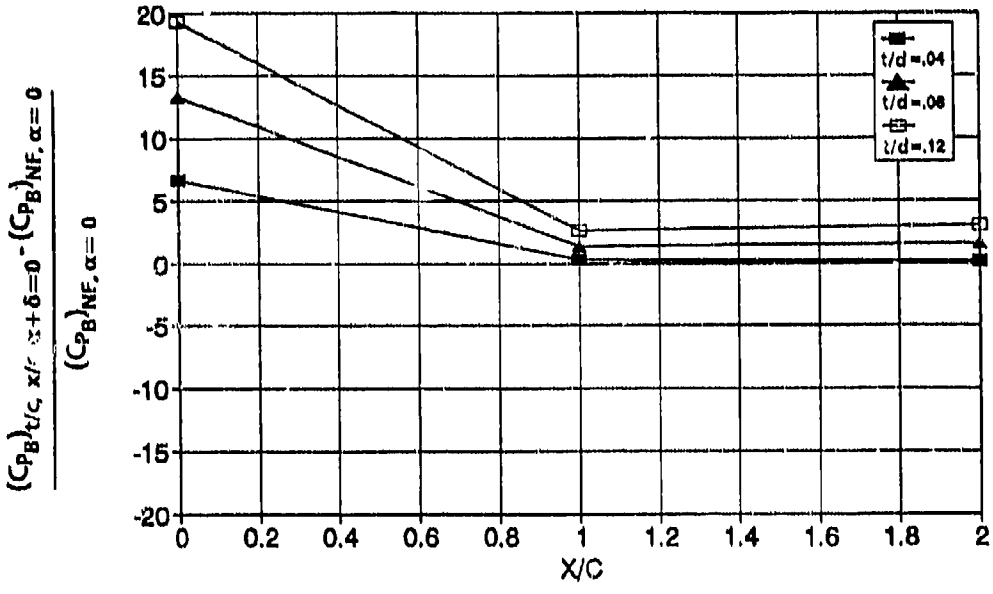

FIGURE 10a. PERCENT INCREASE IN BASE PRESSURE COEFFICIENT DUE TO FIN LOCATION ($|\alpha+\delta|=0°$, $M_\infty=2.0$)

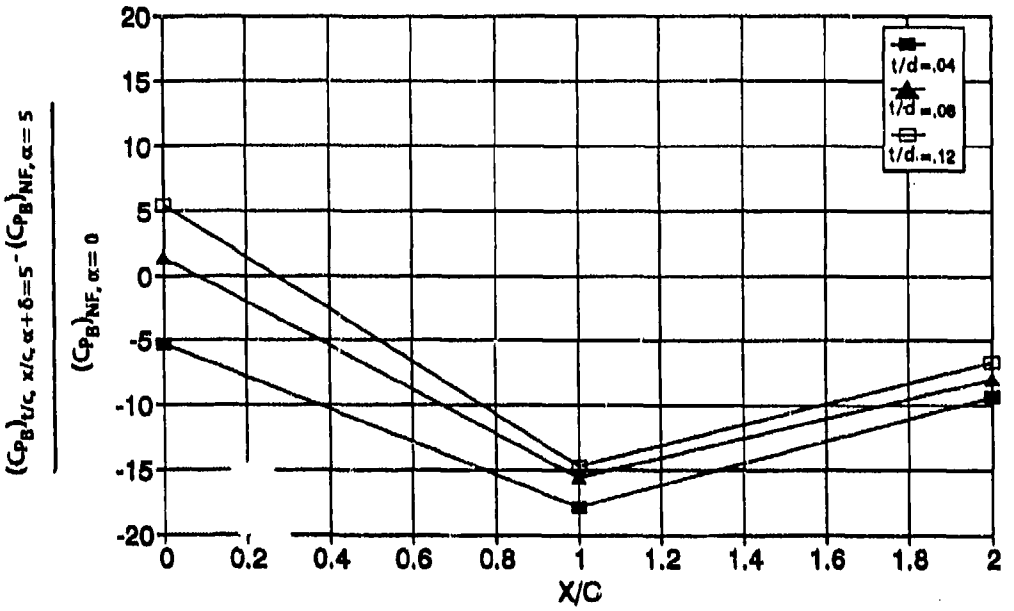

FIGURE 10b. PERCENT INCREASE IN BASE PRESSURE COEFFICIENT DUE TO FIN LOCATION ($|\alpha+\delta| = 5.0°$, $M_\infty = 2.0$)

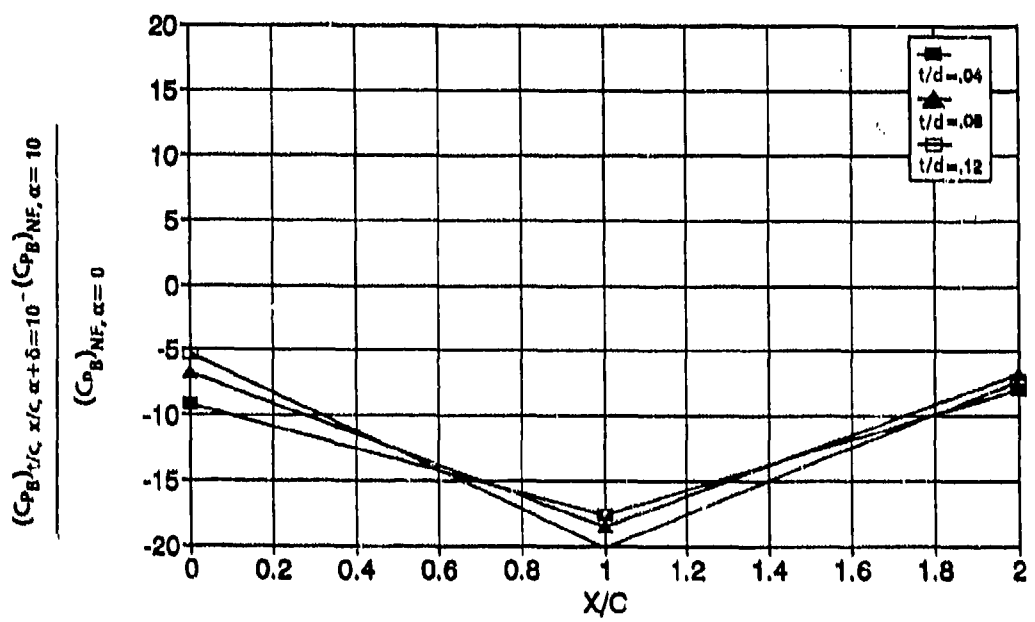

FIGURE 10c. PERCENT INCREASE IN BASE PRESSURE COEFFICIENT DUE TO FIN LOCATION ($|\alpha+\delta| = 10.0°$, $M_\infty = 2.0$)

Once the percent change in C_{P_B} has been determined from Figure 10, the total C_{P_B} is then

$$\left(C_{P_B}\right)_{\alpha, \delta, t/c, x/c} = \left(C_{P_B}\right)_{NF, \alpha} + 0.01\left(\Delta C_{P_B}\right)_{\alpha, \delta, t/c, x/c} \tag{7}$$

Here $(C_{P_B})_\alpha$ is the body-alone base pressure at a given angle of attack and ΔC_{P_B} is the change due to the effect of fins from Figure 10. Note that $(C_{P_B})_{NF, \alpha}$ is calculated by Equation (5). As a result, the effect due to fins and body angle of attack will change from that due to fins in presence of the body when the fins are flush with the base to that of the body alone at angle of attack when the fins are far enough upstream.

Power-on and boattail effects will modify this base pressure coefficient the same as previously discussed.

To summarize the fin location effects, if x/c is close to zero, Equation (6) is used to compute the fin effect on base pressure. If $x/c \neq 0$, a numerical interpolation is used based on Figure 10 where the variables are x/c, t/d, and $|\alpha+\delta|$. The body-alone angle of attack effect is computed by Equation (5). The fin effects on base pressure vary from the values of Equation (6) where $x/c=0$ to those of the body-alone Equation (5) upstream of the base. The total power-off base pressure coefficient is then given by Equation (7). The base pressure coefficient is modified for power-on effects as currently done in the OAP. The base drag including boattail effects is then

$$C_{A_B} = \left(-C_{P_B}\right)_{\alpha, \delta, t/c, x/c}\left(\frac{d}{d_{ref}}\right)^3 \tag{8}$$

4. COMPARISON OF BASE DRAG EMPIRICAL MODELS TO WIND TUNNEL DATA

This section compares the improved empirical base drag prediction model (IAP) with the older version currently in use in the 1981 version of the aeroprediction code (OAP) to wind tunnel data. The data used will be that of the present tests plus those of Reference 26 for low Mach number body-alone angle-of-attack effects.

4.1 BODY-ALONE ANGLE-OF-ATTACK EFFECTS

Figures 11a, b, and c show the results of the IAP and OAP prediction results for body-alone angle-of-attack base pressure for several Mach numbers. The IAP results show improvement over the OAP prediction at all Mach numbers. However, the OAP model, even though it was based on a very sparse amount of data, exhibits the correct trends and is reasonably accurate. The maximum error on C_{P_B} compared to the data

for the OAP was about 20 percent. The IAP model of course duplicates the wind tunnel results just as it was designed to do.

Figures 11a, b, and c further illustrate the fact that the empirical models of the OAP and IAP basically guess as to the behavior of base pressure above $\alpha = 15°$ due to lack of a reliable database. This guess is believed good at $M_\infty \geq 3.5$ but questionable for lower Mach numbers. On the other hand, it is certainly better than assuming no change in base pressure with angle of attack, which is what many engineering codes assume.

4.2 BODY-TAIL CONFIGURATIONS

As already discussed, when there is a tail located in the vicinity of the base, the base pressure is affected due to several parameters. Figure 12 shows the IAP results for C_{P_B} as a function of δ compared to the results of the present test data of Wilcox. Also shown are the OAP results, which are straight lines because the OAP empirical model does not include δ as one of its parameters. Figures 12a and b are for $t/c = 0.05$, Figures 12c and d are for $t/c = 0.10$, and Figures 12e and f are for $t/c = 0.15$. All figures are for $x/c = \alpha = 0$ and ω given for several Mach numbers. For Mach numbers of 2 and greater, the present data are used to compare the OAP and IAP models to. For $M_\infty < 2$, no known good quality data are available so only models are shown. Note that at all Mach numbers (other than $M_\infty = 2$), the IAP represents the available data reasonably well. At $M_\infty = 2$, the empirical model intentionally is slightly higher than the current experimental data for two reasons. First, to use the data of the current tests would cause the IAP curve of Figure 1 to be unsmooth. Second, it is suspected that the values of the present test may be slightly on the low side compared to the OAP curve of Figure 1, which represents a compilation of experimental data from other sources.

Figure 13 compares the base pressure coefficient of the OAP and IAP as a function of t/c for $x/c = 0$, 1.0, and 2.0 and at several Mach numbers. Data of Tables 1 and 2 are shown where available. In examining Figure 13, it is clear that the IAP is superior to the OAP when compared to the Table 1 and 2 data for values of the various parameters that are available. For Mach numbers where data are lacking, it is suspected that the present model is also superior. However additional data are required to substantiate this.

The final case considered is one in which several variables are considered simultaneously. This is generally the situation in actual flight environments. The case considered is for $t/c = 0.15$, $x/c = 1$, and Mach number 2. Base pressure coefficient versus control deflection is given in Figure 14 for the OAP, IAP, and the data of Tables 1 and 2 at $\delta = 0$. Note that the OAP gives only a constant value for C_{P_B} independent of α and δ when fins are present whereas the IAP shows a variation according to the new empirical model for $\alpha = 0$ and 5°. However, for $\alpha = 10°$, no variation is shown because no data are available for $x/c > 0$ where α and δ are both increased. Hence, the

empirical model changes only up to $|\alpha+\delta| \simeq 10°$ when $x/c \succ 0.1$. Above $|\alpha+\delta| = 10°$, no additional change is assumed to occur. Also, note that the main difference between the wind tunnel data and the IAP results is the slight difference in the $(C_{P_B})_{NF,\ \alpha=0}$ body-alone values. The empirical model appears to represent the change in C_{P_B} with combined angle-of-attack and x/c values reasonably well.

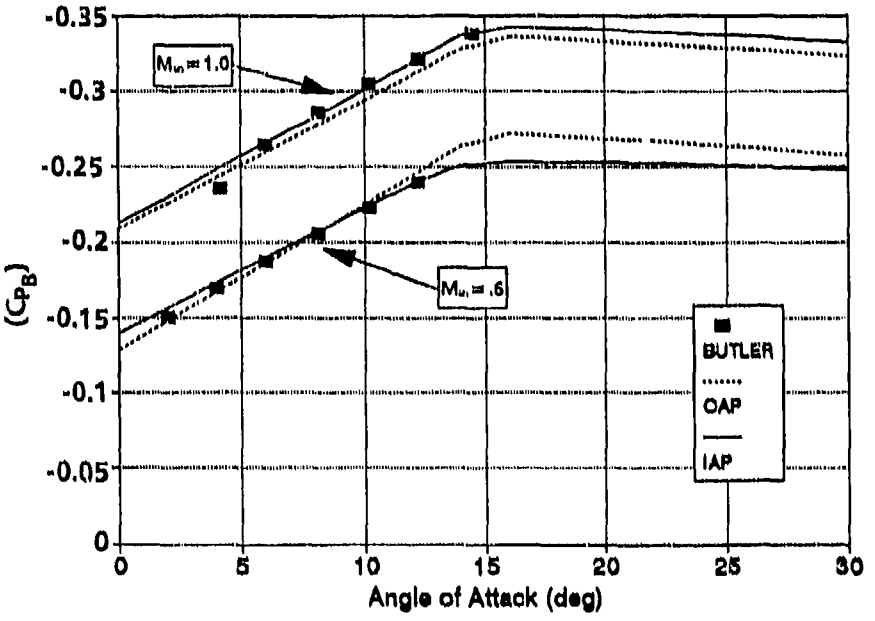

FIGURE 11a. COMPARISON OF BODY-ALONE BASE PRESSURE PREDICTED BY THE OAP AND IAP AS A FUNCTION OF ANGLE OF ATTACK ($M_\infty = 0.6, 1.0$)

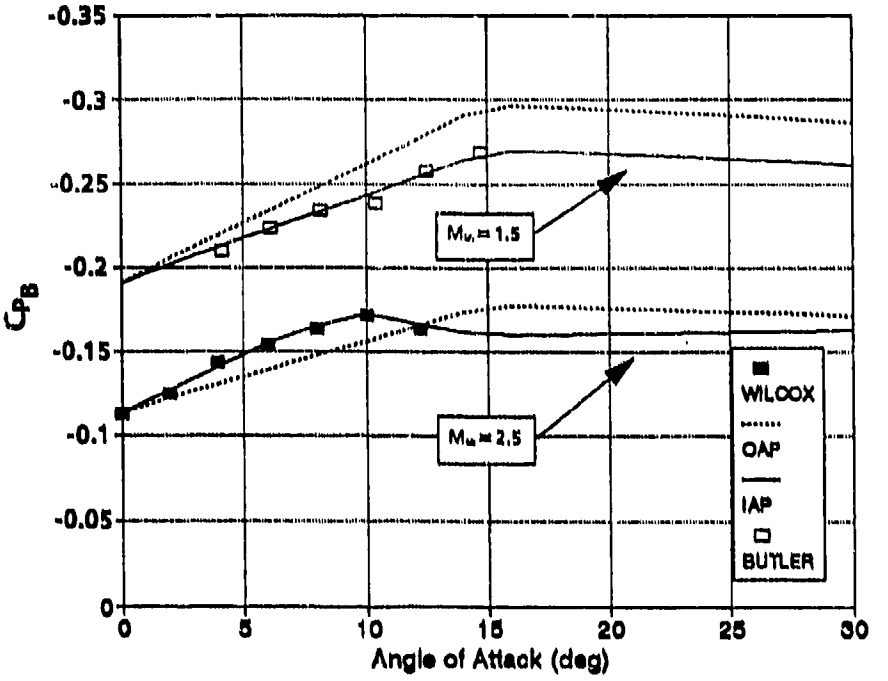

FIGURE 11b. COMPARISON OF BODY-ALONE BASE PRESSURE PREDICTED BY THE OAP AND IAP AS A FUNCTION OF ANGLE OF ATTACK ($M_\infty = 1.5, 2.5$)

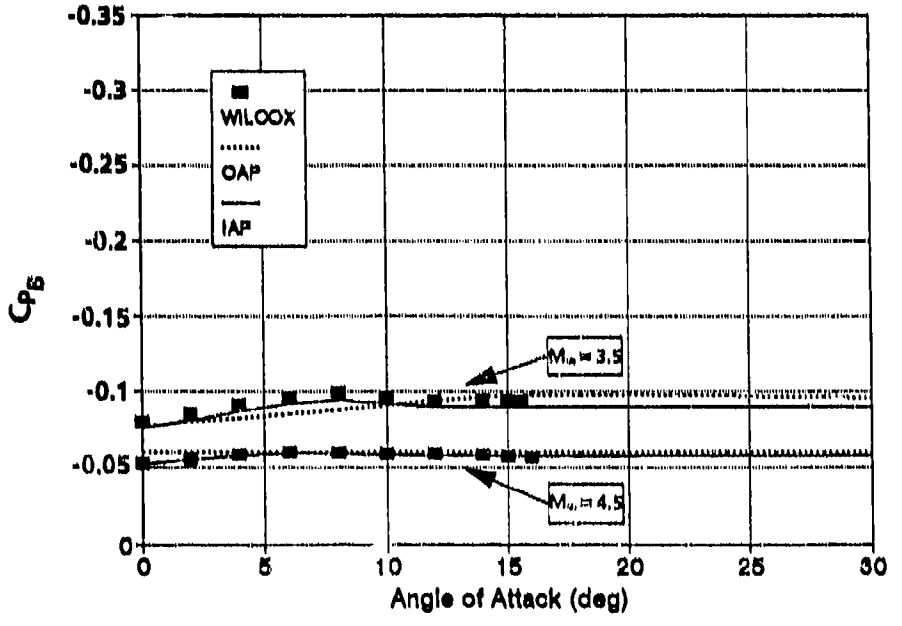

FIGURE 11c. COMPARISON OF BODY-ALONE BASE PRESSURE PREDICTED BY THE OAP AND IAP AS A FUNCTION OF ANGLE OF ATTACK ($M_\infty = 3.5, 4.5$)

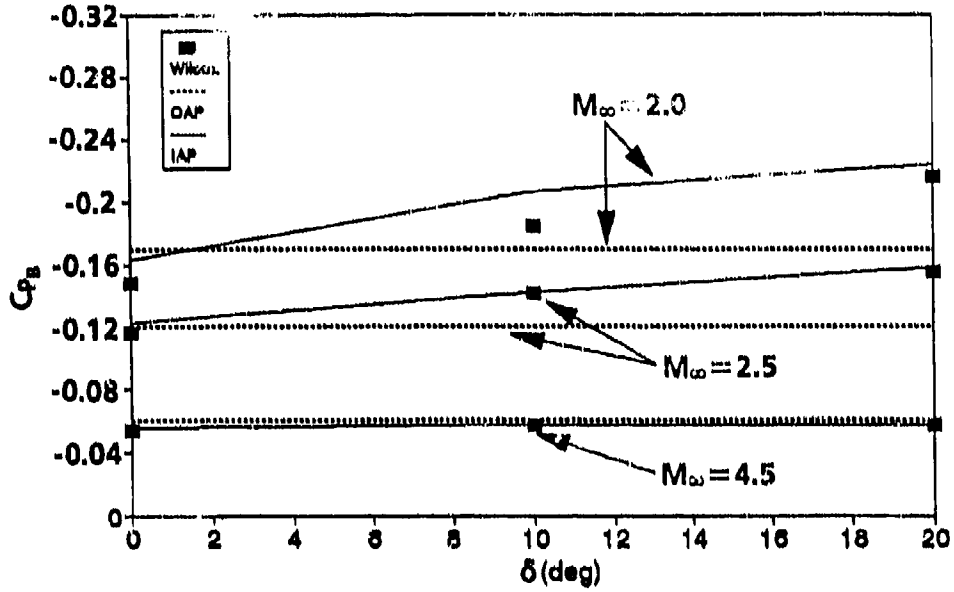

FIGURE 12a. COMPARISON OF BODY-TAIL BASE PRESSURE PREDICTED BY THE OAP AND IAP AS A FUNCTION OF CONTROL DEFLECTION
($t/c = 0.05$; $M_\infty = 2.0, 2.5, 4.5$; $x/c = 0$)

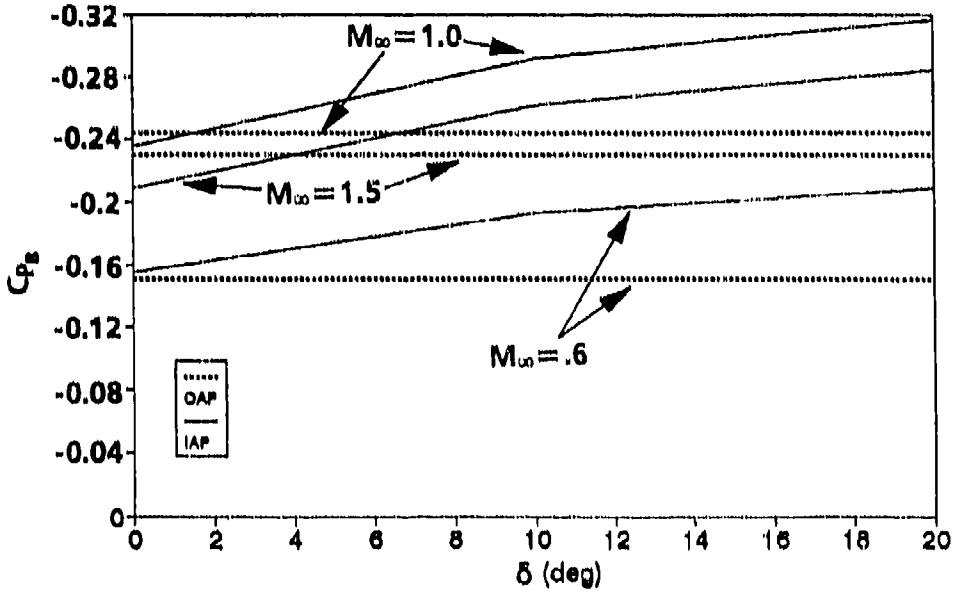

FIGURE 12b. COMPARISON OF BODY-TAIL BASE PRESSURE PREDICTED BY THE OAP AND IAP AS A FUNCTION OF CONTROL DEFLECTION
($t/c = 0.05$; $M_\infty = 0.6, 1.0, 1.5$; $x/c = 0$)

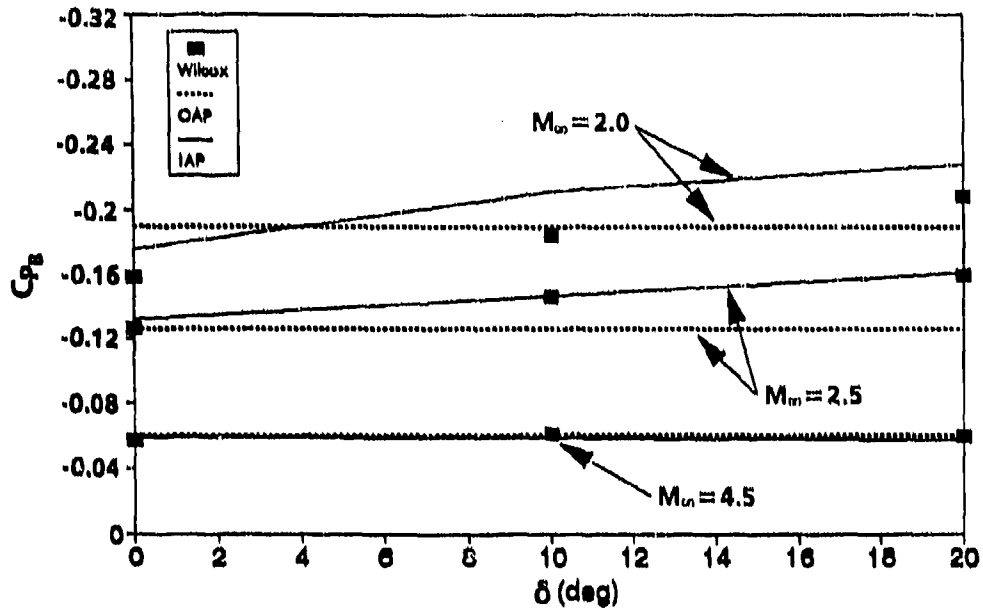

FIGURE 12c. COMPARISON OF BODY-TAIL BASE PRESSURE PREDICTED BY THE OAP AND IAP AS A FUNCTION OF CONTROL DEFLECTION
($t/c = 0.10$; $M_\infty = 2.0, 2.5, 4.5$; $x/c = 0$)

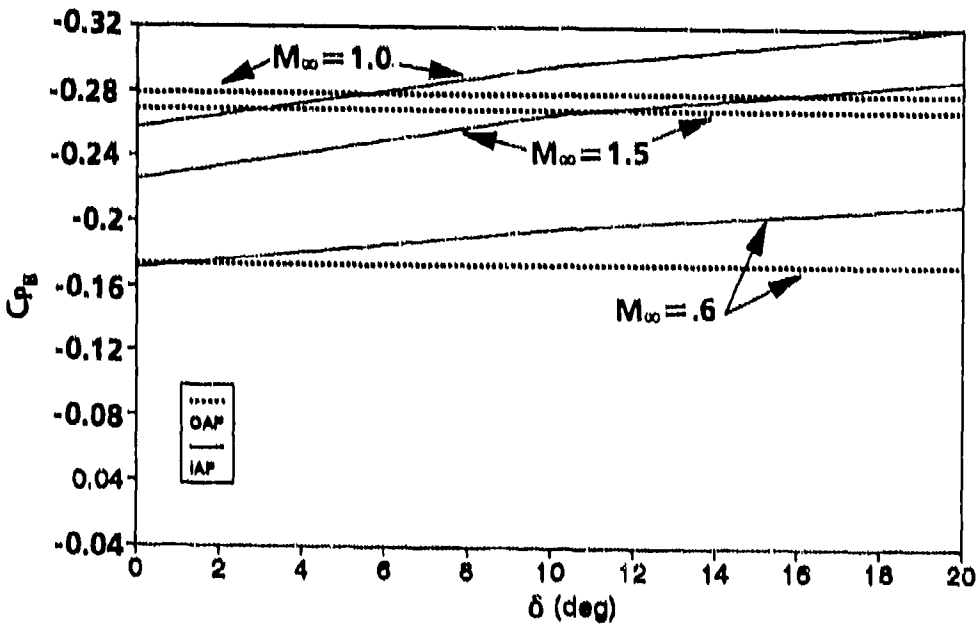

FIGURE 12d. COMPARISON OF BODY-TAIL BASE PRESSURE PREDICTED BY THE OAP AND IAP AS A FUNCTION OF CONTROL DEFLECTION
($t/c = 0.10$; $M_\infty = 0.6, 1.0, 1.5$; $x/c = 0$)

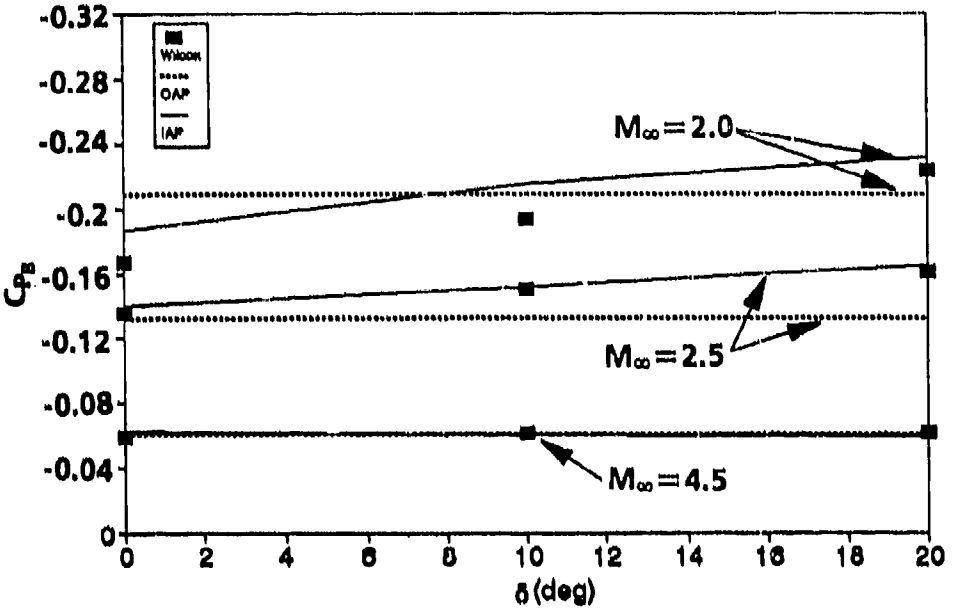

FIGURE 12e. COMPARISON OF BODY-TAIL BASE PRESSURE PREDICTED BY THE OAP AND IAP AS A FUNCTION OF CONTROL DEFLECTION
($t/c = 0.15$; $M_\infty = 2.0, 2.5, 4.5$; $x/c = 0$)

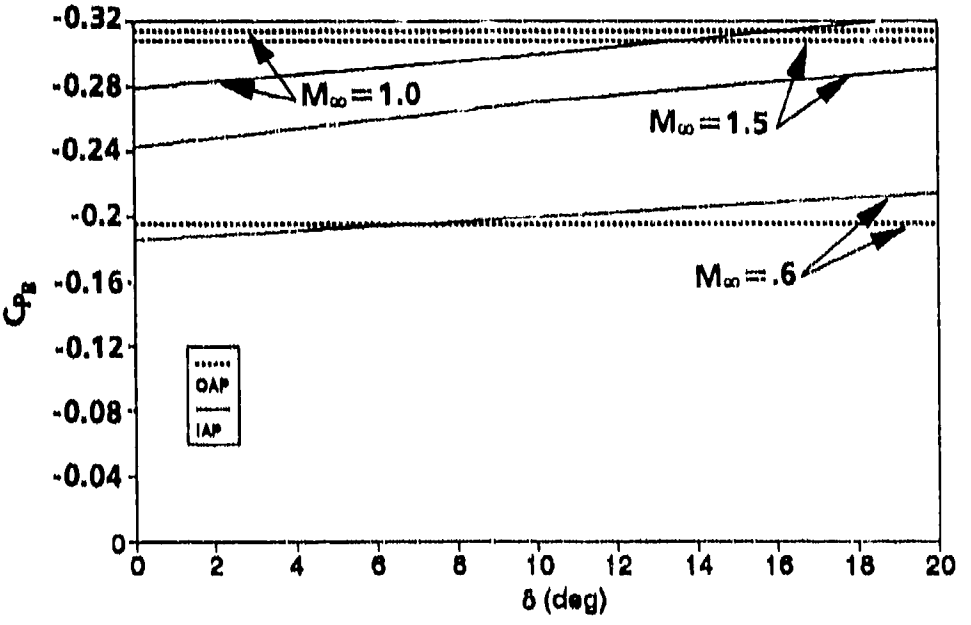

FIGURE 12f. COMPARISON OF BODY-TAIL BASE PRESSURE PREDICTED BY THE OAP AND IAP AS A FUNCTION OF CONTROL DEFLECTION
($t/c = 0.15$; $M_\infty = 0.6, 1.0, 1.5$; $x/c = 0$)

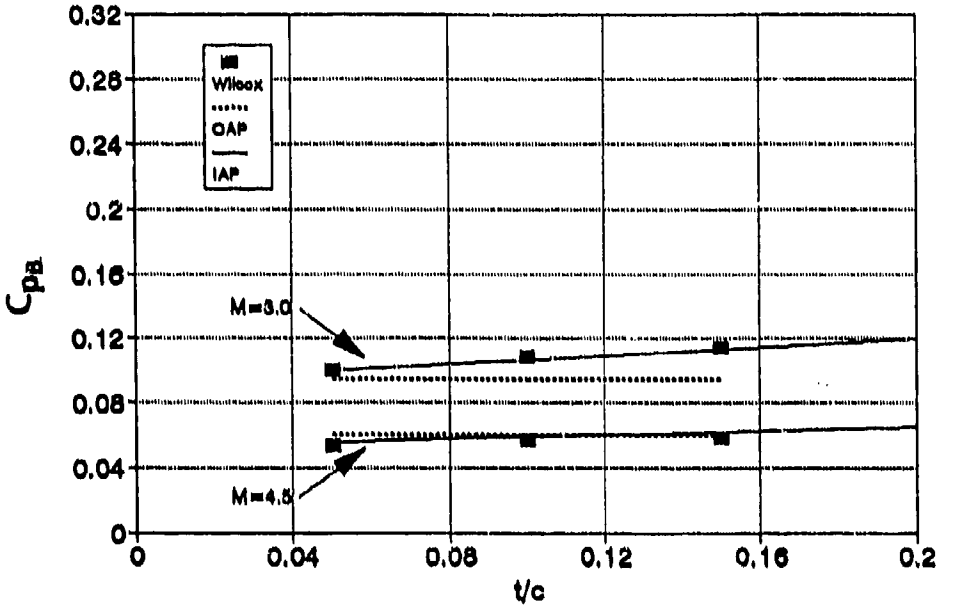

FIGURE 13a. COMPARISON OF BODY-TAIL BASE PRESSURE PREDICTED BY THE OAP AND IAP AS A FUNCTION OF FIN THICKNESS ($\alpha = \delta = 0$; $x/c = 0$; $M_\infty = 3.0, 4.5$)

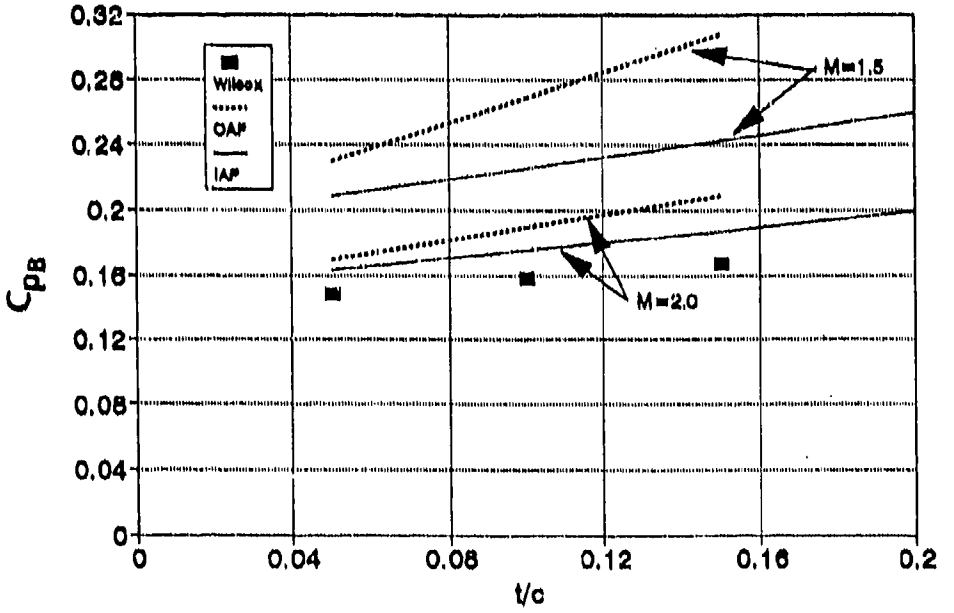

FIGURE 13b. COMPARISON OF BODY-TAIL BASE PRESSURE PREDICTED BY THE OAP AND IAP AS A FUNCTION OF FIN THICKNESS ($\alpha = \delta = 0$; $x/c = 0$; $M_\infty = 1.5, 2.0$)

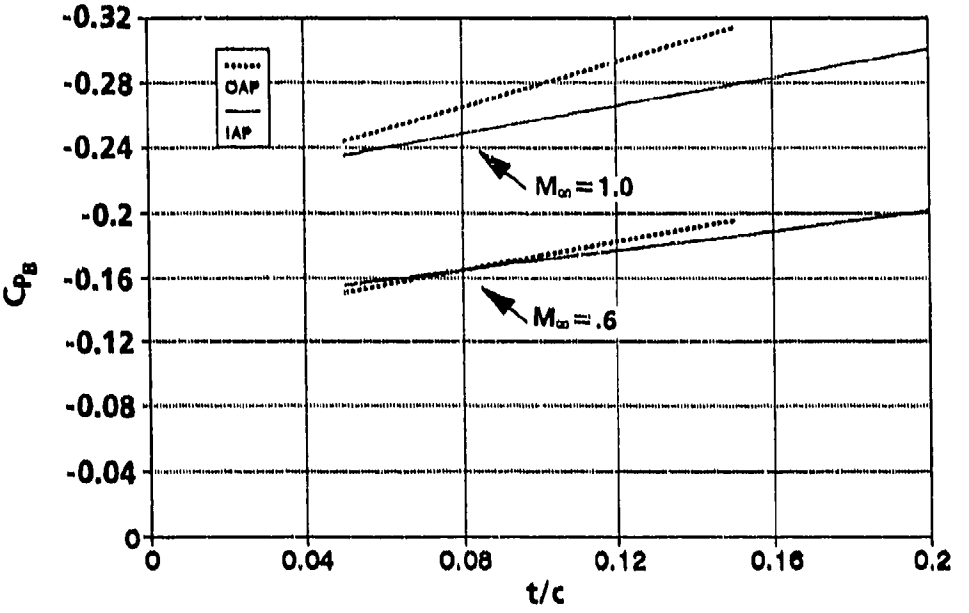

FIGURE 13c. COMPARISON OF BODY-TAIL BASE PRESSURE PREDICTED BY THE OAP AND IAP AS A FUNCTION OF FIN THICKNESS ($\alpha = \delta = 0$; $x/c = 0$; $M_\infty = 0.6, 1.0$)

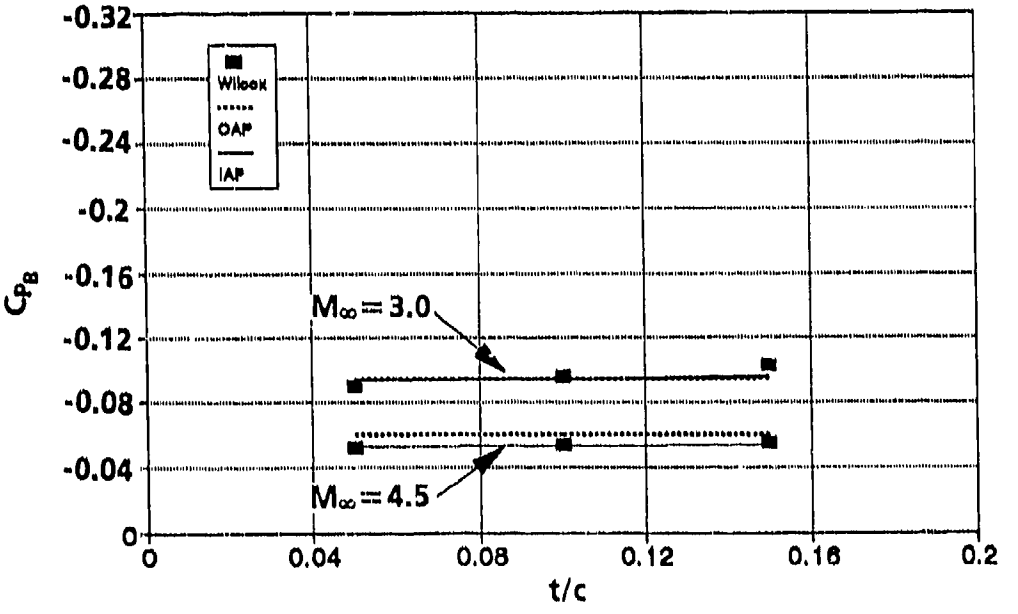

FIGURE 13d. COMPARISON OF BODY-TAIL BASE PRESSURE PREDICTED BY THE OAP AND IAP AS A FUNCTION OF FIN THICKNESS ($\alpha = \delta = 0$; $x/c = 1.0$; $M_\infty = 3.0, 4.5$)

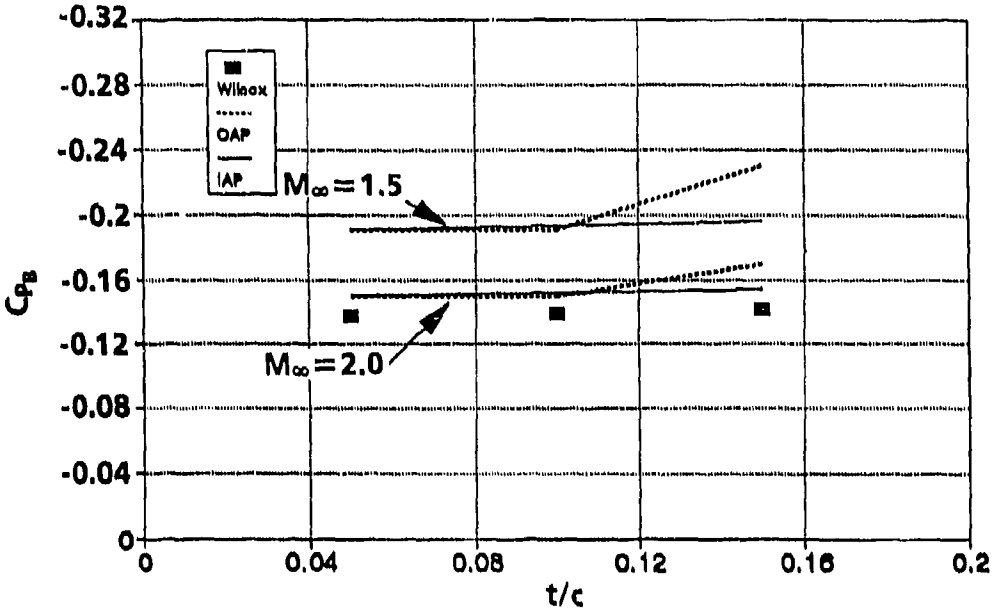

FIGURE 13e. COMPARISON OF BODY-TAIL BASE PRESSURE PREDICTED BY THE OAP AND IAP AS A FUNCTION OF FIN THICKNESS ($\alpha = \delta = 0$; $x/c = 1.0$; $M_\infty = 1.5, 2.0$)

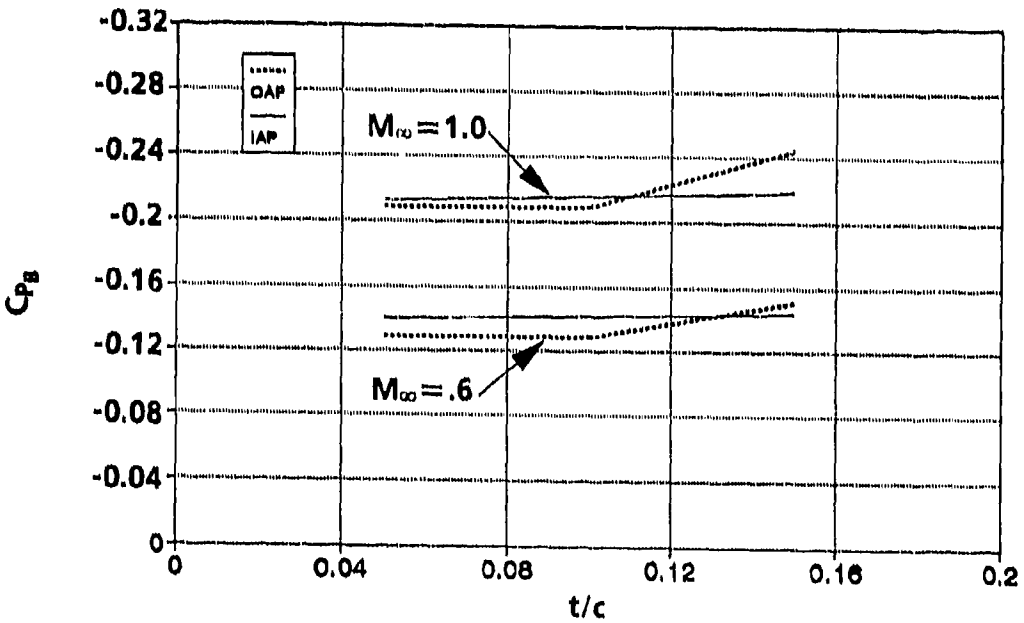

FIGURE 13f. COMPARISON OF BODY-TAIL BASE PRESSURE PREDICTED BY THE OAP AND IAP AS A FUNCTION OF FIN THICKNESS ($\alpha = \delta = 0$; $x/c = 1.0$; $M_\infty = 0.6, 1.0$)

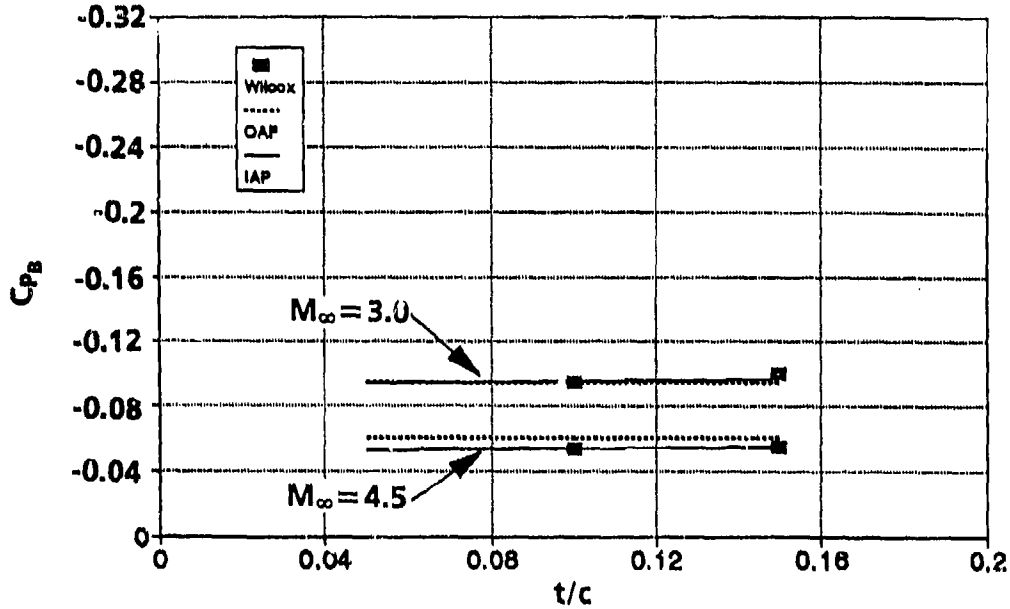

FIGURE 13g. COMPARISON OF BODY-TAIL BASE PRESSURE PREDICTED BY THE OAP AND IAP AS A FUNCTION OF FIN THICKNESS ($\alpha = \delta = 0$; $x/c = 2.0$; $M_\infty = 3.0, 4.5$)

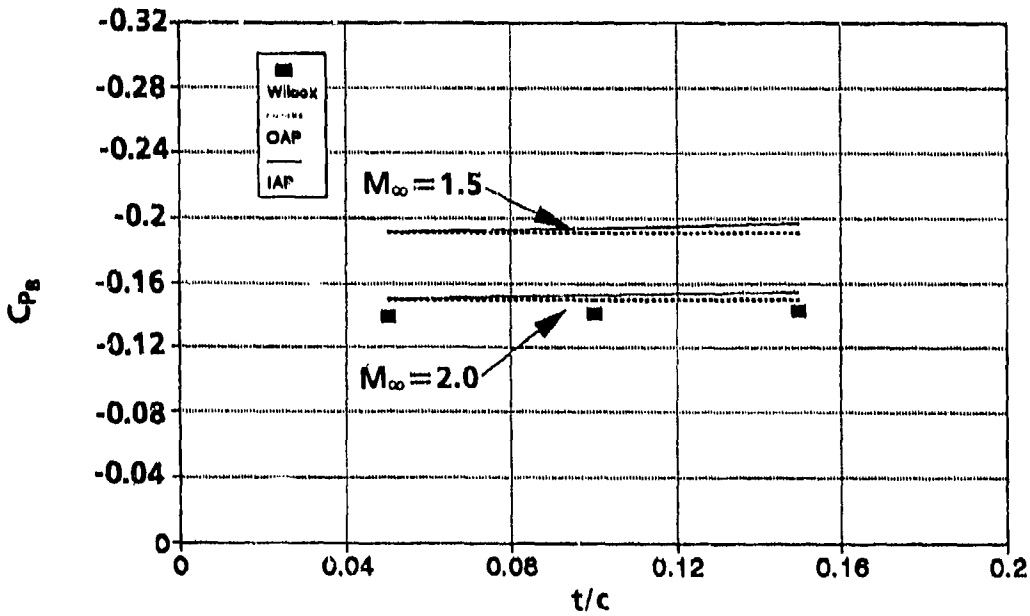

FIGURE 13h. COMPARISON OF BODY-TAIL BASE PRESSURE PREDICTED BY THE OAP AND IAP AS A FUNCTION OF FIN THICKNESS ($\alpha = \delta = 0$; $x/c = 2.0$; $M_\infty = 1.5, 2.0$)

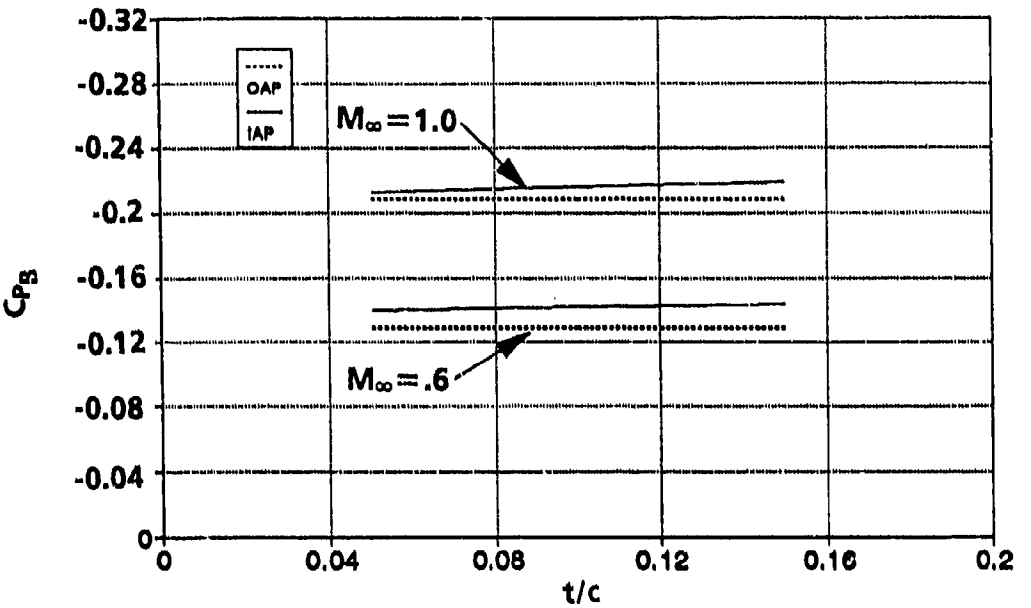

FIGURE 13i. COMPARISON OF BODY-TAIL BASE PRESSURE PREDICTED BY THE OAP AND IAP AS A FUNCTION OF FIN THICKNESS ($\alpha = \delta = 0$; $x/c = 2.0$; $M_\infty = 0.6, 1.0$)

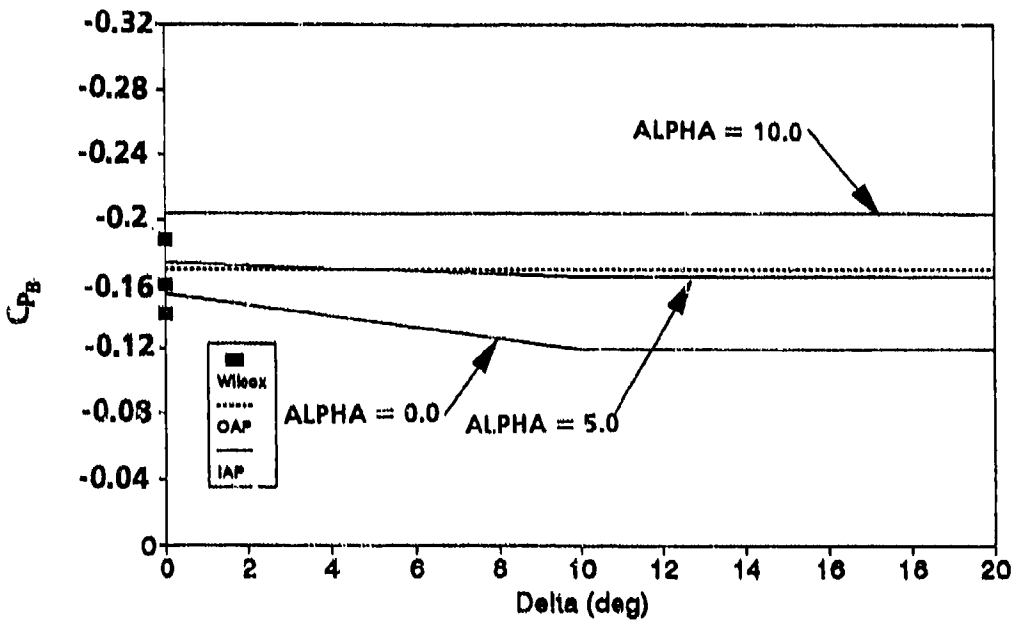

FIGURE 14. COMPARISON OF BODY-TAIL BASE PRESSURE PREDICTED BY THE OAP AND IAP AS A FUNCTION OF CONTROL DEFLECTION AND ANGLE OF ATTACK ($t/c = 0.15$, $x/c = 1.0$, $M_\infty = 2.0$)

5. SUMMARY AND RECOMMENDATIONS

To summarize, new wind tunnel data have been generated to aid in base pressure prediction as a function of body angle of attack, Mach number, fin control deflection, fin thickness, and fin location. Data were taken over a Mach number range of 2 to 4.5, angle of attack of 0° to 16°, fin t/c ratio of 0.05 to 0.15, fin location of flush with the base to two chord lengths ahead of the base, and control deflection of 0° to 20°. At Mach 2, some data were taken with a combination of several of the above variables present whereas at other Mach numbers, only one parameter was changed for a given tunnel condition.

Based on these new data, more recent data from other wind tunnel tests conducted since the empirical base drag model for the OAP was developed in the mid-1970's, and the data from which the empirical model was originally developed, a new and improved empirical base drag prediction model has been developed. This new model is a function of Mach number, angle of attack, fin control deflection, fin thickness, and fin location. In comparison with the OAP and the new wind tunnel data set, it is seen that the IAP reduces the errors of the OAP substantially. Furthermore, the OAP did not account for fin deflection or even angle-of-attack effects if tail fins were present.

While the new model estimates angle-of-attack effects to 30°, control deflection up to 30°, and fin thickness effects for all Mach numbers, in many cases these estimates are based on extrapolations and engineering judgment. As a result, additional wind tunnel data are needed to validate or modify the current model as appropriate. In particular, it is recommended that data be taken for base pressure for the following conditions:

1. body alone: $15 \leq \alpha \leq 30°$; $0 \leq M_\infty \leq 4.5$
2. body tail: fins flush with base; $15° \leq \alpha \leq 30°$; $M_\infty \leq 4.5$
3. body tail: fins flush with base; $\alpha = 0$; $0.05 \leq t/c \leq 0.15$, $0 \leq M_\infty < 2.0$
4. body tail: fins upstream of base; several values of α and δ; one value of t/c; three Mach numbers
5. body tail: more cases where combinations of several parameters are tested simultaneously for use in an empirical model validation

All data taken in future tests should be taken with the same rigor as with the present tests where enough pressure taps are used to get a good average of base pressure for use in base drag computations.

6. REFERENCES

1. Moore, F. G., *Computational Aerodynamics at NAVSWC: Past, Present, and Future*, NAVSWC TR 90-569, October 1990.

2. Devan, L., *Aerodynamics of Tactical Weapons to Mach Number 8 and Angle of Attack 180°: Part I, Theory and Application*, NSWC TR 80-346, October 1980.

3. Devan, L.; and Mason, L., *Aerodynamics of Tactical Weapons to Mach Number 8 and Angle of Attack 180°: Part II, Computer Program and Users Guide*, NSWC TR 81-358, September 1981.

4. Devan, L.; Mason, L.; and Moore, F. G., "Aerodynamics of Tactical Weapons to Mach Number 8 and Angle of Attack 180°," AIAA Paper No. 82-0250, 20th Aerospace Sciences Meeting, Orlando, FL.

5. Love, E. S., *Base Pressure at Supersonic Speeds on Two-Dimensional Airfoils and on Bodies of Revolution with and without Turbulent Boundary Layers*, NACA TN 3819, 1957.

6. Chapman, D. R., *An Analysis of Base Pressure at Supersonic Velocities and Comparison with Experiment*, NACA TR 1051, 1951.

7. Bureau of Naval Weapons, *Handbook of Supersonic Aerodynamics*, NAVWEPS Report 1488, Vol. 3, 1961.

8. Reller, J. O., Jr.; and Hamaker, F. M., *An Experimental Investigation of the Base Pressure Characteristics of Nonlifting Bodies of Revolution at Mach Numbers from 2.73 to 4.98*, NACA TN 3393, 1955.

9. Peck, R. F., *Flight Measurements of Base Pressure on Bodies of Revolution with and without Simulated Rocket Chambers*, NACA TN 3372, 1955.

10. Fraenkel, L. E., *A Note on the Estimation of the Base Pressure on Bodies of Revolution at Supersonic Speeds*, Royal Aircraft Establishment TN No. AERO 2203, 1952.

11. U. S. Army Missile Command, *Engineering Design Handbook: Design of Aerodynamically Stabilized Free Rockets*, AMCP 706-280, 1968.

12. Stoney, W. E., Jr., *Collection of Zero-Lift Data on Bodies of Revolution from Free-Flight Investigations*, NASA TR R-100, 1961.

13. Kurzweg, H. H., "New Experimental Investigations on Base Pressure in the NOL Supersonic Wind Tunnels at Mach Numbers 1.2 to 4.24," NOL Memo 10113, 1950.

14. Heyser, A.; Maurer, F.; and Oberdorffer, E., "Experimental Investigation on the Effect of Tail Surfaces and Angle-of-Attack on Base Pressure in Supersonic Flow," *Conference Proceedings: The Fluid Dynamic Aspects of Ballistics*, AGARD-CP-10, pp. 263-290, 1966.

15. Spahr, J. R.; and Dickey, R. R., *Effect of Tail Surfaces on the Base Drag of a Body of Revolution at Mach Numbers of 1.5 and 2.0*, NACA TN-2360, 1951.

16. Hill, Freeman K.; and Alpher, Ralph A., "Base Pressures at Supersonic Velocities," *Journal of Aeronautical Sciences*, Vol. 16, No. 3, pp. 153-160, March 1949.

17. Brazzel, Charles E.; and Henderson, James H., "An Empirical Technique for Estimating Power-On Base Drag of Bodies-of-Revolution with a Singe Jet Exhaust," *Proceedings*, Specialists Meeting Sponsored by the AGARD Fluid Dynamics Panel, held in Mulhouse, France, 5-8 September 1966.

18. Johnson, L. H., "Approximate Engine-On Base Pressure Computations for Aerodynamic Computer Codes," NSWC K21 Tech. Memo 82-11, March 1982.

19. Moore, F. G., Body Alone Aerodynamics of Guided and Unguided Projectiles at Subsonic, Transonic, and Supersonic Mach Numbers, NWL TR-2796, November 1972.

20. Moore, F. G., *Aerodynamics of Guided and Unguided Weapons: Part I—Theory and Application*, NWL TR-3018, December 1973.

21. Jackson, Charlie M., Jr.; Corlett, William A.; and Monta, William J., *Description and Calibration of the Langley Unitary Plan Wind Tunnel*, NASA TP 1905, 1981.

22. Braslow, Albert L.; and Knox, Eugene C., *Simplified Method for Determination of Critical Height of Distributed Roughness Particles for Boundary-Layer Transition at Mach Numbers from 0 to 5*, NACA TN 4363, 1958.

23. Braslow, Albert L.; Hicks, Raymond M.; and Harris, Roy V., Jr., *Use of Grit-Type Boundary-Layer-Transition Strips on Wind-Tunnel Models*, NASA TN D-3579, 1966.

24. Juanarena, Douglas B., "A Multiport Sensor and Measurement System for Aerospace Pressure Measurements," *Proceedings of the 25th International Instrumentation Symposium*, 1979.

25. NASA Langley Research Center Tri-Service Missile Database, Transmitted from NASA/LaRC Jerry M. Allen to NAVSWC on 5 November 1991 (formal NASA documentation in process).

26. Butler, C; Sears, E.; and Pellas, S., *Aerodynamic Characteristics of 2-, 3-, and 4-caliber Tangent-Ogive Cylinders with Nose Bluffness Ratios of 0.00, 0.25, 0.50, and 0.75 at Mach Numbers from 0.6 to 4.0.*, AFATL-TR-77-8, January 1977.

27. Hill, Freeman K.; and Alpher, Ralph A., *Base Pressure at Supersonic Velocities*, Johns Hopkins University, Bumblebee Report 106, November 1949.

7. SYMBOLS AND DEFINITIONS

A	base area, in.^{2}
$A_1, A_2, A_3, \ldots A_8$	area sections used for weighted base drag coefficient calculations in.^{2} (see Equation 4)
c	fin root chord, in.
C_{A_B}	axial force coefficient due to base pressure
C_{D_B}	base drag coefficient $= (C_{A_B})_{\alpha=0}$
C_{P_B}	base pressure coefficient
C_{p_i}	pressure coefficient, $(p_i - p) / q$
d	body diameter at the body base
d_{ref}	reference diameter
F_1, F_2, F_3	symbols defining parameters used in semiempirical model
M_∞	freestream Mach number
p	freestream static pressure, lb/ft^2
p_i	measured static pressure, lb/ft^2
p_o	stagnation pressure, lb/ft^2

	freestream dynamic pressure, lb/ft^2
	radius, in.
r_b	radius of base, 2.5 in.
R_n	freestream unit Reynolds number per foot
t	fin thickness at root chord, in.
t_{tip}	fin thickness at tip, in.
t/c	fin thickness-to-chord ratio
t/d	fin thickness-to-body reference diameter ratio
T_o	stagnation temperature, °F
x	distance from body base to fin trailing edge (for $\delta = 0°$)
x/c	distance from body base to fin trailing edge (for $\delta = 0°$) in tail root chord lengths
α	body angle of attack (deg) (positive nose up)
δ	fin control deflection (positive leading edge up)
Subscripts on C_{p_B}	
NF	C_{p_B} of body alone with no fins
t/c	C_{p_B} of body with fins of a given thickness-to-chord ratio
x/c	C_{p_B} of body with fins located a given distance from the body base in fin root chord lengths
α	C_{p_B} of body at a given angle of attack
δ	C_{p_B} of body with fins at a given deflection angle

DISTRIBUTION

	Copies
ATTN CODE 20 (SELWYN)	1
CODE 21 (ZIMET)	1
CODE 213 (SIEGEL)	1
CHIEF OF NAVAL RESEARCH	
OFFICE OF NAVAL TECHNOLOGY	
800 N QUINCY ST BCT #1	
ARLINGTON VA 22217-5000	
ATTN CODE 1132F (LEKOUDIS)	1
CODE 12 (WOOD)	1
CODE 121 (HANSEN)	1
CODE 1215 (FEIN)	1
CHIEF OF NAVAL RESEARCH	
OFFICE OF NAVAL RESEARCH	
800 N QUINCY ST BCT #1	
ARLINGTON VA 22217-5000	
ATTN CODE 3591 (PORTER)	1
CODE 3592 (STRUTZ)	1
CODE 3592 (HALTER)	1
TECHNICAL LIBRARY	1
COMMANDER	
NAVAL AIR WARFARE CENTER	
WEAPONS DIVISION	
CHINA LAKE CA 93555-6001	
ATTN TECHNICAL LIBRARY	1
COMMANDER	
NAVAL SEA SYSTEMS COMMAND	
2531 NATIONAL CITY BLDG 3	
WASHINGTON DC 20362-5160	
ATTN AIR-53012D (JOHNSON)	1
RM 904/JP2	
TECHNICAL LIBRARY	1
COMMANDER	
NAVAL AIR SYSTEMS COMMAND	
WASHINGTON DC 20361-5300	
ATTN C KLEIN	1
TECHNICAL LIBRARY	1
COMMANDER	
NAVAL AIR WARFARE CENTER	
WEAPONS DIVISION	
POINT MUGU CA 93042-5000	

	Copies
ATTN T C TAI	1
M J MALIA	1
TECHNICAL LIBRARY	1
COMMANDER	
NAVAL SHIP RESEARCH AND	
DEVELOPMENT CENTER	
WASHINGTON DC 20034	
ATTN R M HOWARD	1
TECHNICAL LIBRARY	1
SUPERINTENDENT	
US NAVAL POSTGRADUATE SCHOOL	
MONTEREY CA 93943-5000	
ATTN S GREENHALGH	1
C REITZ	1
TECHNICAL LIBRARY	1
COMMANDING OFFICER	
NAVAL AIR WARFARE CENTER	
AIRCRAFT DIVISION	
WARMINSTER PA 18974-5000	
ATTN HEAD, WEAPONS DEPT	1
HEAD, SCIENCE DEPT	1
SUPERINTENDENT	
US NAVAL ACADEMY	
ANNAPOLIS MD 21402	
ATTN M KRUMINS	1
TECHNICAL LIBRARY	1
OFFICER IN CHARGE	
NAVAL INTELLIGENCE SUPPORT CENTER	
4301 SUITLAND RD	
WASHINGTON DC 20390	
ATTN CODE 30 (CHILDERS)	1
CHIEF OF NAVAL RESEARCH	
NAVY SDI	
2211 JEFFERSON DAVIS HWY	
RM 810 CP5	
ALEXANDRIA VA 22217	
ATTN PAUL MURAD	1
DIAG/DT-4T	
DEFENSE INTELLIGENCE AGENCY	
WASHINGTON DC 20546	

DISTRIBUTION (CONTINUED)

	Copies
ATTN CODE 50255 (WAGGONER) NAVAL WEAPONS SUPPORT CENTER CRANE IN 47522	1
ATTN CODE 5252P (KRAUSE) TECHNICAL LIRRARY COMMANDER INDIAN HEAD DIVISION NAVAL SURFACE WARFARE CENTER INDIAN HEAD MD 20640-5000	1 1
ATTN TECHNICAL LIBRARY DIRECTOR DEVELOPMENT CENTER MARINE CORPS DEVELOPMENT AND EDUCATION COMMAND QUANTICO VA 22134	1
ATTN M TAUBER TECHNICAL LIBRARY AFATL (ADLRA) (DLGC) EGLIN AFB FL 32542-5000	1 1
ATTN K COBB E SEARS L E LIJEWSKI C COTTRELL TECHNICAL LIBRARY EGLIN AIR FORCE BASE FL 32542	1 1 1 1 1
ATTN TECHNICAL LIBRARY USAF ACADEMY COLORADO SPRINGS CO 80912	1
ATTN G KURYLOWICH D SHEREDA J JENKINS R SAMUELS TECHNICAL LIBRARY COMMANDING OFFICER AFSC WRIGHT--PATTERSON AFB OH 45433	1 1 1 1 1
ATTN TECHNICAL LIBRARY ADVANCED RESEARCH PROJECTS AGENCY DEPARTMENT OF DEFENSE WASHINGTON DC 20305	1
ATTN J USSELTON W B BAKER JR TECHNICAL LIBRARY ARNOLD ENGINEERING DEVELOPMENT CENTER USAF TULLAHOMA TN 37389	1 1 1
ATTN TECHNICAL LIBRARY NASA WASHINGTON DC 20546	1
ATTN M TAUBER TECHNICAL LIBRARY NASA AMES RESEARCH CENTER MOFFETT CA 94035-1099	1 1
ATTN C SCOTT D CURRY NASA JOHNSON SPACE CENTER HOUSTON TX 77058	1 1
ATTN W C SAWYER B HENDERSON D MILLER J ALLEN F WILCOX TECHNICAL LIBRARY NASA LANGLEY RESEARCH CENTER HAMPTON VA 23365	1 1 1 1 5 2
ATTN BILL WALKER DAVE WASHINGTON COMMANDING GENERAL AMSI-RD-SI-AT REDSTONE ARSENAL AL 35898	1 1
ATTN H HUDGINS G FRIEDMAN TECHNICAL LIBRARY COMMANDING GENERAL ARRADCOM PICTINNY ARSENAL DOVER NJ 07801 WASHINGTON DC 20013	1 1 1

DISTRIBUTION (CONTINUED)

	Copies
ATTN C H MURPHY	1
R M McCOY	1
W STUREK	1
C NIETUBICZ	1
A MIKHAIL	1
P PLOSTINS	1
TECHNICAL LIBRARY	1
COMMANDING GENERAL	
BALLISTIC RESEARCH LABORATORY	
ABERDEEN PROVING GROUND	
MD 21005	
ATTN CODE TNC (BLACKLEDGE)	1
CDR AL KOREJO	1
DIRECTOR	
INTERCEPTOR TECHNOLOGY	
STRATEGIC DEFENSE INITIATIVE	
THE PENTAGON	
WASHINGTON DC 20350	
ATTN SFAE-SD-ASP	1
SFAE-SD-HED	1
DEPUTY COMMANDER	
US ARMY STRATEGIC DEFENSE	
COMMAND	
PO BOX 1500	
HUNTSVILLE AL 35807-3801	
ATTN PROF J A SCHETZ	1
VIRGINIA POLYTECHNIC AND	
STATE UNIVERSITY	
DEPT OF AEROSPACE ENGINEERING	
BLACKSBURG VA 24060	
ATTN F R DeJARNETTE	1
NORTH CAROLINA STATE UNIVERSITY	
DEPT OF MECHANICAL AND	
AEROSPACE ENGINEERING	
BOX 7921	
RALEIGH NC 27695	
ATTN J M WU	1
C BALASUBRAMAYAN	1
TECHNICAL LIBRARY	1
THE UNIVERSITY OF TENNESSEE	
SPACE INSTITUTE	
TULLAHOMA TN 37388	

	Copies
ATTN R NELSON	1
TECHNICAL LIBRARY	1
UNIVERSITY OF NOTRE DAME	
DEPT OF AEROSPACE AND	
MECHANICAL ENGINEERING	
BOX 537	
NOTRE DAME IN 46556	
ATTN E LUCERO	1
L TISSERAND	1
D FROSTBUTTER	1
TECHNICAL LIBRARY	1
APPLIED PHYSICS LABORATORY	
JOHNS HOPKINS UNIVERSITY	
JOHNS HOPKINS RD	
LAUREL MD 20707-6099	
ATTN D G MILLER	1
TECHNICAL LIBRARY	1
LAWRENCE LIVERMORE LAB	
EARTH SCIENCES DIVISION	
UNIVERSITY OF CALIFORNIA	
LIVERMORE CA 94550	
ATTN F PRILLMAN	1
W B BROOKS	1
R STANCIL	1
VOUGHT CORPORATION	
PO BOX 5907	
DALLAS TX 75222	
ATTN TECHNICAL LIBRARY	1
HUGHES AIRCRAFT CORPORATION	
CANOGA PARK CA 91304	
ATTN DR WALTER RUTLEDGE	1
R LaFARGE	1
R EISLER	1
WALTER RUTLEDGE (1635)	1
TECHNICAL LIBRARY	1
SANDIA NATIONAL LABORATORIES	
ALBUQUERQUE NM 87185-5800	
ATTN TECHNICAL LIBRARY	1
MARTIN MARIETTA AEROSPACE	
PO BOX 5837	
ORLANDO FL 32805	

DISTRIBUTION (CONTINUED)

	Copies
ATTN S SOPCZAK	1
TECHNICAL LIBRARY	1
HONEYWELL INC 600 SECOND ST MINNEAPOLIS MN 55343	
ATTN B OMILIAN	1
CAL SPAN ADVANCED TECHNOLOGY CENTER PO BOX 400 BUFFALO NY 14225	
ATTN TECHNICAL LIBRARY	1
ROCKWELL INTERNATIONAL MISSILE SYSTEMS DIVISION 4300 E FIFTH AVE PO BOX 1259 COLUMBUS OH 43216	
ATTN R CAVAGE	1
ADVANCED SYSTEMS DESIGN DEPT 113-407 (GB14) ROCKWELL NORTH AMERICAN AIRCRAFT OPERATIONS PO BOX 92098 LOS ANGELES CA 90009	
ATTN G H RAPP	1
MOTOROLA INC MISSILE SYSTEMS OPERATIONS 3201 E McDOWELL RD PO BOX 1417 SCOTTSDALE AZ 85252	
ATTN R WYRICK	1
BOEING COMPUTER SERVICES INC PO BOX 24346 SEATTLE WA 98124	

	Copies
ATTN J XERIKOS	1
N CAMPBELL	1
TECHNICAL LIBRARY	1
McDONNELL-DOUGLAS ASTRONAUTICS CO (WEST) 5301 BOLSA AVE HUNTINGTON BEACH CA 92647	
ATTN J WILLIAMS	1
S VUKELICH	1
J FIVEL	1
R GERBSCH (CODE 1111041)	1
TECHNICAL LIBRARY	1
McDONNELL-DOUGLAS ASTRONAUTICS CO (EAST) BOX 516 ST LOUIS MO 63166-0516	
ATTN M DILLENIUS	1
NIELSEN ENGINEERING AND RESEARCH INC 510 CLYDE AVE MOUNTAIN VIEW CA 95043	
ATTN DR M FINK	1
UNITED TECHNOLOGIES NORDERN SYSTEMS MAIL STOP K041 NORWALK CT 06856	
ATTN T LUNDY	1
D ANDREWS	1
TECHNICAL LIBRARY	1
LOCKHEED MISSILES AND SPACE CO INC PO BOX 1103 HUNTSVILLE AL 35807	
ATTN L E ERICSSON	1
P REDING	1
TECHNICAL LIBRARY	1
LOCKHEED MISSILES AND SPACE CO INC PO BOX 504 SUNNYVALE CA 94086	

DISTRIBUTION (CONTINUED)

	Copies
ATTN M WAREHAM RAYTHEON MISSILE SYSTEMS 50 APPLE HILL DR STOP T2SA9 TEWKSBURY MA 01876-0901	1
ATTN LLOYD PRATT AEROJET TACTICAL SYSTEMS CO PO BOX 13400 SACRAMENTO CA 95813	1
ATTN KURT HIVELY GENERAL DYNAMICS/CONVAIR PO BOX 85357 SAN DIEGO CA 92138	1
ATTN SAM BLACK GOODYEAR AEROSPACE CORP 1210 MASSILLON RD AKRON OH 44315	1
ATTN W NORDGREN/721 GOULD INC OSD 18901 EUCLID AVE CLEVELAND OH 44117	1
ATTN DR Y C SHEN AEROJET ELECTRO SYSTEMS CO PO BOX 296-III AZUSA CA 91702	1
ATTN PETROS KYPRIOS TEXAS INSTRUMENTS INC PO BOX 405 MAIL STOP 3408 LOUISVILLE TX 75067	1
ATTN GERMAN MILITARY REP US/OA GMR TRAFFIC AND TRANSPORTATION DIVISION 10 SERVICE RD DULLES INTERNATIONAL AP WASHINGTON DC 20041	1
ATTN DORIA GLADSTONE BATTELLE MEMORIAL INSTITUTE COLUMBUS DIVISION 505 KING AVE COLUMBUS OH 43201-2693	1
ATTN DR T P SHIVANANDA TRW ONE SPACE PARK REDONDO BEACH CA 90278	1
ATTN K C LEE ACCUREX CORP PO BOX 7040 520 CLYDE AVE MOUNTAIN VIEW CA 94039	1
ATTN A CHABOKI FMC CORPORATION 1300 S SECOND ST PO BOX 59043 MINNEAPOLIS MN 55450-0043	1
ATTN L FRENCH TRACOR AEROSPACE AUSTIN INC 6500 TRACO LANE AUSTIN TX 87825	1
ATTN ASO/LO-IS ISRAEL AIR FORCE LIAISON OFFICER 700 ROBBINS AVE PHILADELPHIA PA 19111	1
ATTN W J CLARK DYNA EAST CORPORATION 3132 MARKET ST PHILADELPHIA PA 19104	1
ATTN D SCHMITZ CHAMBERLAIN MANUFACTURING CORP RESEARCH AND DEVELOPMENT DIVISION PO BOX 2545 WATERLOO IA 50704-2545	1

DISTRIBUTION (CONTINUED)

	Copies
ATTN BRIAN WALKUP HERCULES AEROSPACE PRODUCT CO ALLEGHANY BALLISTIC LAB ROCKET CENTER WV 26726	1
ATTN ASSISTANT DEFENSE COOPERATION ATTACHE EMBASSY OF SPAIN WASHINGTON DC 20016	1
ATTN J FORKOIS KAMAN SCIENCES CORP 1500 GARDEN OF THE GODS RD PO BOX 7463 COLORADO SPRINGS CO 80933	1
ATTN M R D'ANGELO MIT LINCOLN LABORATORY LEXINTON NA 02173-0073	1
ATTN M S MILLER DYNETICS INC PO DRAWER B HUNTSVILLE AL 35814-5050	1
ATTN H A McELROY GENERAL DEFENSE CORP PO BOX 127 RED LION PA 17356	1
ATTN R SEPLAK BRUNSWICK CORP DEFENSE DIVISION 3333 HARBOR BLVD COSTA MESA CA 92628-2009	1
ATTN J W McDONALD GENERAL RESEARCH CORP ADVANCED TECHNOLOGY INC 5383 HOLLISTER AVE PO BOX 6770 SANTA BARBARA CA 93160-6770	1
ATTN CAROL BUTLER OTI INTERNATIONAL 60 2ND ST SUITE 301 PO BOX 37 SHALIMAR FL 32579	1
ATTN ARMAMENT SYSTEMS DEPT GENERAL ELECTRIC CO BURLINGTON VT 05401	1
ATTN JACK GRAMS TELEDYNE RYAN AERONAUTICAL 2701 HARBOR DR SAN DIEGO CA 92138	1
ATTN DR T LIN TRW ELECTRONICS AND DEFENSE SECTOR BLDG 527/RM 706 PO BOX 1310 SAN BERNADINO CA 92402	1
ATTN B S PRATS AIRTHERMOPHYSICS GENERAL ELECTRIC CO 3198 CHESTNUT ST PHILADELPHIA PA 19104	1
ATTN G VINCENT SPARTA INC 4301 CORPORATE DR HUNTSVILLE AL 35805	1
ATTN D P FORSMO TECHNICAL LIBRARY RAYTHEON COMPANY MISSILE SYSTEMS DIVISION HARTWELL RD BEDFORD MA 01730	1 1
ATTN S PEARLSING P GIRAGOSIAN RAYTHEON COMPANY SPENCER LABORATORY BOX SL7162 BURLINGTON MA 01803	1 1
ATTN NEILL S SMITH ARAP 1950 OLD GALLOWS RD SUITE 302 VIENNA VA 22180	1

DISTRIBUTION (CONTINUED)

	Copies
ATTN T R PEPITONE AEROSPACE TECHNOLOGY INC PO BOX 1809 DAHLGREN VA 22448	1
ATTN WILLIAM FACINELLI ALLIED SIGNAL PO BOX 22200 MS 1230-21E TEMPE AZ 85285	1
ATTN CDR R TEMPEST BRITISH NAVY STAFF WASHINGTON DC 20008	1
ATTN DENNIS BROWN NATIONAL AERONAUTICAL ESTAB NATIONAL RESEARCH COUNCIL MONTREAL RD OTTOWA ON CANADA K1A0R6	1
ATTN J EVANS DREV PO BOX 8800 COURCELETTE PQ CANADA GOA 1RO	1
ATTN H G KNOCHE DR GREGORIOU MESSERSCHMIDT-BOLKOW-BLOHM GMBH UNTERNEHMENSBEREICH APPARATE MUNCHEN 80-POSTFACH 801149 BAYERN FED REP OF GERMANY (DFR)	1 1
ATTN DR DONALD SPRING AEROSPACE ENGINEERING DEPT AUBURN UNIVERSITY AL 36849-5338	1
ATTN BOB WHYTE ARROW TECH ASSOCIATES INC 1233 SHELBURNE RD D-8 SO BURLINGTON VT 05403	1
ATTN FU HO LING 1300 30TH ST APT E2-31 BOULDER CO 80303	1
ATTN PROF H F NELSON DEPT OF MECH AND AERO ENG UNIVERSITY OF MISSOUR-ROLLA ROLLA MO 65401	1
DEFENSE TECHNICAL INFORMATION CENTER CAMERON STATION ALEXANDRIA VA 22314	12
ATTN GIFT AND EXCHANGE DIVISION LIBRARY OF CONGRESS WASHINGTON DC 20390	1
GIDEP OPERATIONS OFFICE CORONA CA 91720	1
DEFENSE PRINTING SERVICE WASHINGTON NAVY YARD WASHINGTON DC 20374	1

INTERNAL DISTRIBUTION	
C	1
D	1
D1	1
D2	1
D4	1
A	1
B	1
E	1
E231	3
E232	2
E261 (GREEN)	1
E32 (GIDEP)	2
F	1
G	1
G02	1
G04	10
G05	1
G06	1
G07	1
G20	1
G205	1
G23	1
G23 (CHADWICK)	1

	Copies
G23 (DEVAN)	1
G23 (HARDY)	1
G23 (HYMER)	1
G23 (McINVILLE)	1
G23 (ROWLES)	1
G23 (WEISEL)	1
G30	1
G40	1
G42 (CRAFF)	1
G50	1
G60	1
G80	1
G90	1
GHO	1
GH3	1
K	1
K	1
K10	1
K20	1
K204	1
N	1
R	1
R44	1
R44 (PRIOLO)	1
R44 (HSIEH)	1
R44 (WARDLAW)	1

REPORT DOCUMENTATION PAGE

Form Approved
OMB No. 0704-0188

1. AGENCY USE ONLY *(Leave blank)*	2. REPORT DATE	3. REPORT TYPE AND DATES COVERED
	October 1992	Final

4. TITLE AND SUBTITLE
Improved Empirical Model for Base Drag Prediction on Missile Configurations Based on New Wind Tunnel Data

5. FUNDING NUMBERS

6. AUTHOR(S)
Frank G. Moore Floyd Wilcox (NASA/LaRC) Tom Hymer

7. PERFORMING ORGANIZATION NAME(S) AND ADDRESS(ES)
Naval Surface Warfare Center
Dahlgren Division
Dahlgren, VA 22448-5000

8. PERFORMING ORGANIZATION REPORT NUMBER
NSWCDD/TR-92/509

9. SPONSORING/MONITORING AGENCY NAME(S) AND
Surface-launched Weapons Technology Block Program
Office of Naval Research

10. SPONSORING/MONITORING AGENCY REPORT NUMBER

11. SUPPLEMENTARY NOTES

12a. DISTRIBUTION/AVAILABILITY
Approved for public release; distribution is unlimited.

12b. DISTRIBUTION CODE

13. ABSTRACT *(Maximum 200 words)*

New wind tunnel data have been taken, and a new empirical model has been developed for predicting base drag on missile configurations. The new wind tunnel data were taken at NASA/LaRC in the Unitary Plan Wind Tunnel at Mach numbers from 2.0 to 4.5, angles of attack to 16°, fin control deflections up to 20°, fin thickness-to- chord (t/c) ratio of 0.05 to 0.15, and fin locations flush with the base to two chord lengths upstream of the base.

The newly developed empirical model uses these data along with previous wind tunnel data. It estimates base drag as a function of all the above variables along with boattail and power-on or power-off effects. In comparing the new empirical model to that used in the former aeroprediction code, the new model gives improved accuracy over wind tunnel data. The new model also is more robust due to inclusion of additional variables. On the other hand, additional wind tunnel data are needed to validate or modify the current empirical model in areas where data are not available.

14. SUBJECT TERMS			15. NUMBER OF PAGES
empirical model base drag prediction	missile configuration	wind tunnel	52 16. PRICE CODE

17. SECURITY CLASSIFICATION OF REPORT	18. SECURITY CLASSIFICATION OF THIS PAGE	19. SECURITY CLASSIFICATION OF ABSTRACT	20. LIMITATION OF ABSTRACT
UNCLASSIFIED	UNCLASSIFIED	UNCLASSIFIED	UL

GENERAL INSTRUCTIONS FOR COMPLETING SF 298

The Report Documentation Page (RDP) is used in announcing and cataloging reports. It is important that this information be consistent with the rest of the report, particularly the cover and its title page. Instructions for filling in each block of the form follow. It is important to ***stay within the lines*** to meet ***optical scanning requirements.***

Block 1. Agency Use Only *(Leave blank)*.

Block 2. Report Date. Full publication date including day, month, and year, if available (e.g. 1 Jan 88). Must cite at least the year.

Block 3. Type of Report and Dates Covered. State whether report is interim, final, etc. If applicable, enter inclusive report dates (e.g. 10 Jun 87 - 30 Jun 88).

Block 4. Title and Subtitle. A title is taken from the part of the report that provides the most meaningful and complete information. When a report is prepared in more than one volume, repeat the primary title, add volume number, and include subtitle for the specific volume. On classified documents enter the title classification in parentheses.

Block 5. Funding Numbers. To include contract and grant numbers; may include program element number(s), project number(s), task number(s), and work unit number(s). Use the following labels:

C	- Contract	PR	- Project
G	- Grant	TA	- Task
PE	- Program Element	WU	- Work Unit Accession No.

BLOCK 6. Author(s). Name(s) of person(s) responsible for writing the report, performing the research, or credited with the content of the report. If editor or compiler, this should follow the name(s).

Block 7. Performing Organization Name(s) and address(es). Self-explanatory.

Block 8. Performing Organization Report Number. Enter the unique alphanumeric report number(s) assigned by the organization performing the report.

Block 9. Sponsoring/Monitoring Agency Name(s) and Address(es). Self-explanatory.

Block 10. Sponsoring/Monitoring Agency Report Number. *(If Known)*

Block 11. Supplementary Notes. Enter information not included elsewhere such as: Prepared in cooperation with...; Trans. of...; To be published in.... When a report is revised, include a statement whether the new report supersedes or supplements the older report.

Block 12a. Distribution/Availability Statement. Denotes public availability or limitations. Cite any availability to the public. Enter additional limitations or special markings in all capitals (e.g. NOFORN, REL, ITAR).

DOD	- See DoDD 5230.24, "Distribution Statements on Technical Documents."
DOE	- See authorities.
NASA	- See Handbook NHB 2200.2
NTIS	- Leave blank

Block 12b. Distribution Code.

DOD	- Leave blank.
DOE	- Enter DOE distribution categories from the Standard Distribution for Unclassified Scientific and Technical Reports.
NASA	- Leave blank.
NTIS	- Leave blank.

Block 13. Abstract. Include a brief ***(Maximum 200 words)*** factual summary of the most significant information contained in the report.

Block 14. Subject Terms. Keywords or phrases identifying major subjects in the report.

Block 15. Number of Pages. Enter the total number of pages.

Block 16. Price Code. Enter appropriate price code ***(NTIS only)***

Block 17.-19. Security Classifications. Self-explanatory. Enter U.S. Security Classification in accordance with U.S. Security Regulations (i.e., UNCLASSIFIED). If form contains classified information, stamp classification on the top and bottom of this page.

Block 20. Limitation of Abstract. This block must be completed to assign a limitation to the abstract. Enter either UL (unlimited or SAR (same as report). An entry in this block is necessary if the abstract is to be limited. If blank, the abstract is assumed to be unlimited.